OPTICAL POWER MEASUREMENTS: APPLICATIONS IN FIBER OPTICS AND ULTRAVIOLET RADIOMETRY
Doctoral Dissertation

Jouni Envall

Helsinki University of Technology
Department of Electrical and Communications Engineering
Metrology Research Institute

OPTICAL POWER MEASUREMENTS: APPLICATIONS IN FIBER OPTICS AND ULTRAVIOLET RADIOMETRY
Doctoral Dissertation

Jouni Envall

Helsinki University of Technology
Department of Electrical and Communications Engineering
Metrology Research Institute

Teknillinen korkeakoulu
Sähkö- ja tietoliikennetekniikan osasto
MIKES TKK Mittaustekniikka

HELSINKI UNIVERSITY OF TECHNOLOGY	ABSTRACT OF DOCTORAL DISSERTATION
P. O. BOX 1000, FI-02015 TKK	
http://www.tkk.fi	

Author	Jouni Tapani Envall

Name of the dissertation

Optical Power Measurements: Applications in Fiber Optics and Ultraviolet Radiometry

Abstract

The work described in this thesis has concentrated on development and characterization of detectors, measurement setups and measurement methods for the needs of optical metrology in the fields of fiber optics and ultraviolet (UV) radiometry.

A straightforward detector design for fiber optic power measurements, consisting of a single InGaAs photodiode, has been introduced. The simple and cost effective detectors were found applicable in high-precision measurements at <1-mW level with a combined measurement uncertainty of 0.9% (k=2).

Another detector type for fiber optic power measurements, consisting of an integrating sphere and an InGaAs photodiode, has been characterized for measurements at power levels up to 200 mW. Further characterizations have extended the power range up to 650 mW. The measurement uncertainty of the detector is 0.8% at 1-mW level and 1.3% at 100-mW level (k=2). The capability for accurate measurements of fiber optic power at 100-mW level has been found useful in studying the non-linear properties of optical fibers.

A high-intensity spectral comparator facility for measurements of spectral irradiance responsivity $s(\lambda)$ at UV is presented. The setup consists of a single grating monochromator and an intense xenon source. The high power levels are needed to obtain sufficient signal levels in narrow-band (1 nm) spectral measurements with broadband UV detectors. The power levels obtained were high enough even for measurements at UVB region (280-315 nm).

A sophisticated method for calibration of broadband detectors was tested. The method is based on the measured $s(\lambda)$ of the detector. This method enables the irradiance responsivity of the detector to be calculated for any source whose spectral shape is known. The consistency between this method and the widely used spectroradiometric method was shown.

A novel method for inter-comparisons of calibration facilities of broadband UV detectors is introduced. The method is based on the known $s(\lambda)$ and angular response of the detector. The applicability of the method was verified with a successful inter-comparison between five laboratories.

Tekijä   Jouni Tapani Envall

Väitöskirjan nimi

Optisen tehon mittaukset: sovellukset kuituoptiikassa ja ultraviolettialueen radiometriassa

Käsikirjoituksen jättämispäivämäärä 18.4.2006	Väitöstilaisuuden ajankohta 30.6.2006
☐ Monografia	☒ Yhdistelmäväitöskirja (yhteenveto + erillisartikkelit)

Osasto   Sähkö- ja tietoliikennetekniikan osasto

Laboratorio   MIKES TKK Mittaustekniikka

Tutkimusala   Mittaustekniikka

Vastaväittäjä(t)   Prof. Mario Blumthaler

Työn valvoja   Prof. Erkki Ikonen

(Työn ohjaaja)   TkT Petri Kärhä

Tiivistelmä

Tässä väitöskirjassa kuvatussa tutkimustyössä on keskitytty kuituoptiikassa ja ultraviolettialueen (UV) radiometriassa tarvittavien tehomittarien (detektorien), mittausjärjestelmien ja mittausmenetelmien kehittämiseen.

Tässä työssä on kuvattu yksinkertainen ja edullinen, pelkästä InGaAs-fotodiodista koostuva, kuituoptinen detektori. Tarkat karakterisointimittaukset osoittivat detektorin käyttökelpoiseksi mittanormaaliksi kuituoptisiin tarkkuustehomittauksiin <1 mW tehotasoilla. Detektorin mittausepävarmuus on 0.9% (k=2).

Olemme karakterisoineet integroivasta pallosta ja InGaAs-fotodiodista koostuvan pallodetektorin, ja osoittaneet, että detektori kykenee luotettaviin kuituoptisen tehon mittauksiin aina 200 mW tehotasoille asti. Myöhemmät laboratoriossamme tehdyt mittaukset ovat vielä entisestään laajentaneet tehoaluetta 650 mW asti. Mittausepävarmuus 1 mW tasolla on 0.8% ja 100 mW tasolla 1.3% (k=2). Korkeiden tehotasojen (~100 mW) tarkkuusmittaukset ovat huomattavasti edesauttaneet laboratoriossamme tehtäviä kuitujen epälineaarisia ominaisuuksia käsitteleviä tutkimuksia.

Työssä on esitelty suuritehoinen mittausjärjestelmä UV-alueen detektorien spektrisen irradianssivasteen $s(\lambda)$ mittaamiseen. Järjestelmä koostuu yksihilaisesta monokromaattorista ja suuritehoisesta ksenonlampusta. Korkeat tehotasot edesauttavat laajakaistaisten UV-mittarien spektrisiä mittauksia kapeilla 1 nm kaistoilla. Tehotasot todettiin riittäviksi jopa lyhytaaltoisella UVB-alueella (280-315 nm).

Kokeilimme myös uutta menetelmää laajakaistaisten UV-mittarien kalibrointiin. Menetelmä perustuu $s(\lambda)$:n mittaamiseen. Tätä menetelmää käyttäen voidaan mittarin vaste määrittää mille tahansa lähteelle, jonka spektrimuoto tunnetaan. Osoitimme myös yhtäpitävyyden tämän menetelmän ja laajalti käytetyn spektroradiometrisen menetelmän välillä.

Esittelemme lisäksi uuden menetelmän kansainvälisiin laajakaistaisten UV-mittareiden vertailuihin. Menetelmä hyödyntää mitattua $s(\lambda)$:aa, lisäksi tarvitaan mittarin mitattu kulmavaste. Menetelmän toimivuus on todennettu järjestämässämme kansainvälisessä pilottivertailussa, jonka tulokset esitetään tässä väitöskirjassa.

Asiasanat   optinen teho, mittanormaali, kalibrointi, kuituoptiikka, ultravioletti, spektrinen irradianssivaste

Preface

The research described in this thesis has been carried out at the Metrology Research Institute, Department of Electrical and Communications Engineering of Helsinki University of Technology during the years 2000 – 2006.

I wish to thank the head of Department, professor Pekka Wallin and the head of the laboratory, professor Erkki Ikonen for the possibility to conduct scientific research on the field of optical metrology.

I also wish to thank all the co-authors of the publications of the thesis for contributing to my thesis work.

A very special acknowledgement goes to Dr Petri Kärhä, for guiding me through the system, from an under-graduate student all the way to the doctoral degree, thank you. Also Dr Farshid Manoocheri is acknowledged for his valuable assistance during these years. The whole personnel of the Metrology Research Institute is thanked for all the madness and fun. Especially I would like to thank Dr Markku Vainio, Dr Mart Noorma and M. Sc. Antti Lamminpää. Never change, fellows. The skilful craftsmanship of Mr Seppo Metsälä, while machining most of the mechanics needed in the detectors, is greatly appreciated.

The preliminary examiners of the thesis, professor Esko Kyrö and professor Oleg Okhotnikov, are thanked for their efforts.

Amsterdam, oh Amsterdam...

Centre for Metrology and Accreditation (MIKES), Nordtest, the National Graduate School of Electronics Manufacturing and Tekniikan Edistämissäätiö (TES) are acknowledged for funding the research.

One special acknowledgement is saved for my mathematics teacher, Sakari Salonen from Kaurialan lukio, who ignited the enthusiasm towards mathematical sciences in me.

I have thanked my parents and all the heavy metal bands of the world already in two theses. Well, thanks again.

Absolutely no acknowledgement is given for TCH Snooker. Tack för ingenting. Long live Drunken Sparrow!

Espoo, April 2006

Jouni Envall

List of publications

This thesis consists of an overview and the following selection of the author's publications.

I.   J. Envall, P. Kärhä, and E. Ikonen, "Measurements of fibre optic power using photodiodes with and without an integrating sphere," *Metrologia* **41**, 353-358 (2004).

II.   J. Envall, A. Andersson, J.C. Petersen, and P.Kärhä, "Realization of the scale of high fiber optic power at three national standards laboratories," *Applied Optics* **44**, 5013-5017 (2005).

III.   J. Envall, P. Kärhä, and E. Ikonen, "Calibration of broadband ultraviolet detectors by measurement of spectral irradiance responsivity," *Review of Scientific Instruments* (in press).

IV.   J. Envall, L. Ylianttila, H. Moseley, A. Coleman, M. Durak, P. Kärhä, and E. Ikonen, "Investigation of comparison methods for UVA irradiance responsivity calibration facilities," *Metrologia* **43**, S27-S30 (2006).

Author's contribution

All publications are results of team work of the contributing scientists.

The manuscripts for all the publications have been prepared by the author.

The author constructed the detectors described in Publication I. All the characterization measurements and calibrations, as well as most of the data analysis, have been performed by the author.

The author contributed to the planning of the research described in Publication II. All the measurements and data analysis from TKK's part were performed by the author.

The measurement setup described in Publication III was constructed by the author. The author also prepared all the software needed. The author performed all the characterization measurements and calibrations with the setup. All data analysis were performed by the author.

The author contributed to the planning of the research described in Publication IV. He performed all the measurements and data analysis as the representative of the pilot laboratory.

List of symbols

a	Fiber core radius	n_2	Non-linear refractive index
A	Area	n_2/A_{eff}	Non-linearity coefficient
A_{eff}	Effective area of fiber core	OH$^-$	Hydroxyl ion
c	Speed of light	p	Semiconductor doped with positively charged impurities
c_0	Speed of light in vacuum	P	Power
C	Angular correction	P_{ang}	Angular power distribution
C_{ang}	Cosine correction	pin	pn junction with non-doped layer in between
C_j	Junction capacitance	R	Responsivity
D	Diode	$R'(\theta)$	Measured cosine response
e	Elementary charge	R_{ang}	Measured angular response
$\mathbf{E}$	Electric field	R_s	Series resistance
$\tilde{\mathbf{E}}$	Fourier transform of $\mathbf{E}$	R_{sh}	Shunt resistance
E	Photon energy	S	Quantity of broadband effect
E_g	Band gap energy	$s(\lambda)$	Spectral irradiance responsivity
$E(\lambda)$	Spectral irradiance	$s_{act}(\lambda)$	Actinic function
Ge	Germanium	Si	Silicon
h	Planck's constant	SiO$_2$	Silicon dioxide, silica
$\mathbf{H}$	Magnetic field	T	Thermodynamic temperature
$\tilde{\mathbf{H}}$	Fourier transform of $\mathbf{H}$	u	Uncertainty
I	Current	Ω	Solid angle
I_{dk}	Dark current	ε	Permittivity
I_{ph}	Photocurrent	ε_0	Permittivity of vacuum
I_{tot}	Output current of photodiode	ε_r	Relative permittivity
InGaAs	Indium gallium arsenide	$\varepsilon(\lambda)$	Internal quantum efficiency
InP	Indium phosphate	λ	Wavelength
k	Boltzmann constant	θ	Angle
k	Coverage factor	$\rho(\lambda)$	Spectral reflectance
n	Semiconductor doped with negatively charged impurities	ω	Angular frequency
n	Refractive index		

List of abbreviations

C-band	"conventional" wavelength band 1530 – 1565 nm
CGPM	Conférence Générale des Poids et Mesures
DFM	Danish Fundamental Metrology
DWDM	Dense Wavelength Division Multiplexing
EDFA	Erbium Doped Fiber Amplifier
FOPM	Fiber Optic Power Meter
IR	Infrared
L-band	"long" wavelength band 1565 – 1625 nm
LS	Line source method
MIKES	Centre for Metrology and Accreditation
MRI	Metrology Research Institute
NIR	Near-infrared
OP.DI.MA	Optically Diffuse Reflectance Material
S-band	"short" wavelength band 1460 – 1530 nm
SI	Système Internationale d'Unités (Internat. System of Units)
SIR	Spectral irradiance responsivity method
SOA	Semiconductor Optical Amplifier
SP	Swedish National Testing and Research Institute
SR	Spectroradiometric method
STUK	Radiation and Nuclear Safety Authority
TCH	Terrible Cueball Handling
TKK	Helsinki University of Technology
TUBITAK-UME	National Metrology Institute of Turkey
UV	Ultraviolet
UVA	Part of the UV region; 315 – 400 nm
UVB	Part of the UV region; 280 – 315 nm
UVPD	UV photodiode
WDM	Wavelength Division Multiplexing

Table of contents

1 Introduction

1.1 Background

It would be impossible to imagine the modern world, with all the achievements of science and technology surrounding us, without accurate, reliable measurements of different physical quantities. The scientific discipline that concentrates on studying and developing measurement methods is called metrology. Conférence Générale des Poids et Mesures (CGPM) is the highest international authority in metrology. CGPM has defined the seven base units of the International System of Units (Système Internationale d'Unités, the SI system). [1] On the national level, national standards laboratories realize and maintain scales, or units, for different quantities. The realization of a unit must be traceable to the definition of the unit, to other units and/or to natural constants. Metrology Research Institute of Helsinki University of Technology (TKK) is the Finnish national standards laboratory for the measurements of optical quantities. The institute was appointed by the Centre for Metrology and Accreditation (MIKES) in 1996.

The SI system includes one optical base unit, candela. It is the unit of luminous intensity. The first photometric and radiometric scales were based on sources. The very first scales utilized sources like candles, flames or incandescent filament lamps. [2] The first well-defined physical source, that could be realized anywhere in the world, was introduced in 1948. At that time the definition of candela was based on the radiation of a blackbody radiator in the freezing temperature of platinum. [3] This method of realization did not spread widely, due to the difficulties in operating blackbodies and their high price.

Over the past few decades, the detector-based scales have gained in popularity. The main reason for this development is the introduction of the cryogenic absolute radiometer in 1985. [4] Cryogenic absolute radiometers are nowadays in wide use as the primary standards of optical power in many national standards laboratories, including TKK. [5, 6, 7, 8] Another factor in the popularity of detector-based scales was the introduction of trap detectors. [9, 10, 11] Trap detector is a structure of several photodiodes, used to trap light inside the structure. It can be used as an accurate measurement standard for optical power measurements. The spectral responsivity of a silicon trap detector can be modeled over a wide wavelength range, covering the visible region and parts of ultraviolet (UV) and infrared (IR) radiation. [12]

Optical fiber technology has changed the world as we know it. The huge growth of the Internet would not have been possible, if copper wires had been the most sophisticated tool of the telecommunications community. Internet traffic has experienced exponential growth; it is said to double every four to six months. [13] The applicable bandwidth of copper wires remains under 1 GHz, while the obtainable bandwidth of silica (SiO_2) fiber is 25 THz. [14] At 1-GHz signal modulation speed the attenuation of a copper coaxial cable is 50 dB/km. Lowering the modulation speed down to 1 MHz the copper cable still attenuates the signal 2.5 dB/km. These numbers pale in comparison next to the attenuation of high-quality silica fiber; 0.25 dB/km.

In the metrological point of view, measuring the power of the light propagating in an optical fiber is a complicated task that requires understanding of the special characteristics of the fibers, detectors and methods used. [15, 16, Publication I] Accurate measurements of fiber optic power are essential in characterizing various optical properties of fibers and fiber optic components. [17, 18] Various kinds of detectors have been developed during the past decades. [15, 16, 19, 20, 21, Publication I] In recent years, several national standards laboratories have extended their scales of fiber optic power to higher power levels; up to hundreds of milliwatts or even several watts. [22, Publication II] A need for accurate measurements at such high power levels is a natural consequence of the high transmission powers used in telecommunication networks.

Accurate measurements of ultraviolet (UV) radiation are needed in several fields of science and technology, ranging from space research into medicine, photobiology and ozone research. [23, 24, 25, 26, 27, 28] Also, UV radiation is utilized in many industrial applications, for example, to modify the surface properties of materials [29] or to disinfect foodstuff or drinking water. [30] In many applications the quantity of interest is the total amount of radiation over a wide wavelength band. Often this total, or spectrally integrated, radiation is weighted with a specific actinic function, describing the spectral dependence of a certain effect. This effect may be a photobiological phenomenon, such as erythema of skin [31] or different types of skin cancer. [25] Specific detectors exist for direct measurements of such effects. These detectors – called broadband detectors – produce an electrical signal that, in theory, is proportional to the effect in question. This is achieved by matching the spectral responsivity of the detector with the desired actinic function. Calibration of broadband detectors is complicated. Especially, if the user of the detector is not aware of the limitations of the device, drastic discrepancies may occur. [32] The most significant limitation of broadband detectors is the source dependence of their responsivity. [32, 33, Publication III] Furthermore, inter-comparisons of such detectors and the respective scales of national standards laboratories have proven difficult. Unsuccessful inter-comparisons with huge discrepancies have been reported. [34]

1.2 Progress in this work

The work described in this thesis has concentrated on improving the measurement capabilities in the fields of fiber optic power and broadband UV measurements.

Publication I describes the construction and characterization of detectors to be used as reference standards in fiber optic power measurements. In this study a straightforward design, consisting of a plain InGaAs photodiode, was tested as a reference standard in high-precision metrology. This robust and moderately priced detector design was found applicable for use as a working standard. In addition, another type of detector was built and characterized. This design consisted of an integrating sphere and an InGaAs photodiode. Typically sphere detectors of this kind have one entrance port, which can be equipped with a fiber adapter. The problem with this structure is that when the fiber adapter is removed to allow the absolute calibration of the detector with an open air laser beam, the measurement geometry is different from that used in fiber measurements, when the connector is attached. Several methods have been

14

introduced to overcome this problem. [21, 35] In Publication I we present a novel method to measure quantitatively the error caused by the change in geometry.

The transmitted power used in modern optical networks can be as high as 1 W. This has caused many national standards laboratories to extend their measurements of fiber optic power into higher power levels. In Publication II we discuss the issues that are to be taken into account when performing such extension. Also, the scales of high fiber optic power of TKK, Swedish National Testing and Research Institute (SP) and Danish Fundamental Metrology (DFM) are presented. A trilateral comparison was arranged between the three institutes to compare the scales. The results of the comparison are also given in Publication II.

Publication III describes a measurement setup for measurement of spectral irradiance responsivity $s(\lambda)$ of broadband UV detectors. The measured $s(\lambda)$ can be used to calculate the responsivity of the detector to any radiation source whose spectral shape is known. We were able to show that this setup, consisting of a single grating monochromator and an intense xenon arc lamp, can produce irradiance levels high enough for spectral measurements with broadband sources even at UVB wavelengths (280 – 315 nm). We also demonstrate the agreement of this calibration method with another widely used method, the spectroradiometric calibration.

The calibration method described in Publication III can be used as the basis of a novel method of inter-comparisons of calibration facilities of broadband UV detectors. This method is presented in Publication IV. Because different laboratories participating in the comparison use different sources, methods, and measurement geometries, their measurement results vary by definition. [32, Publication III] To compensate for the systematic deviations due to these issues, the pilot laboratory calculates individual reference values for each laboratory. In order to do this, the pilot laboratory needs the measured $s(\lambda)$ and the angular response of the detector. In addition, the spectra of the sources used, as well as the descriptions of the different measurements geometries are needed. We tested the sensitivity of the method to errors in spectral data, provided by the participants. The method was found very insensitive to such errors. Publication IV also presents the results of an international pilot comparison, in which this novel method was successfully tested.

2   Measuring optical power

2.1   Scale realization

The scale of optical power at most national standards laboratories is currently based on the cryogenic absolute radiometer. The cryogenic absolute radiometer is the most accurate device for measurement of optical power at the moment. [4, 5, 7, 8] It is a so-called electrically calibrated substitution radiometer. The operating principle of such detectors is to heat the absorber of the radiometer in turn with the incident radiation and with an electrical heater. A mechanical shutter is used to block the incident radiation while heating with the electrical heater. When a thermodynamic equilibrium is achieved, i.e. when the temperature of the absorber remains constant, the optical power of the incident radiation is equal to the electrical power of the heater. The electrical power can be measured with low uncertainty. Cryogenic absolute radiometer is an electrically calibrated substitution radiometer, whose absorbing cavity is cooled to the temperature of liquid helium (~4 K) to maximize its sensitivity and to minimize its response time and thermal noise. The relative overall uncertainty of the optical power measurement may be as low as a few parts in 10^5. [8]

2.2   Measurement standards

2.2.1   Thermal detectors and quantum detectors

In principle, any object or device, that produces a measurable physical response when interacting with electromagnetic energy, can be considered a detector. In terms of science and technology, we furthermore demand that the response must be a recordable signal, with known relation to the measured property – typically power – of the radiation. Most detectors used in optical radiation measurements are either thermal detectors or quantum detectors.

The principle of operation of a thermal detector is to sense the heat produced by the incident radiation. The device has an absorber, whose task is to absorb radiation with high efficiency over a wide wavelength band. The absorbance of the absorber is maximized with the correct choice of material used to construct or coat the absorber. Also the shape of the absorber has significance, cavity-shaped absorbers are utilized in many devices. The change in temperature, caused by the absorbed radiation, of the absorber is then measured with some suitable technique. The division between different thermal detectors is based on the technique that is used to detect this temperature change. Cryogenic absolute radiometer, pyroelectric radiometer, thermocouple, thermopile, bolometer and Golay cell are examples of different thermal detectors.

Pyroelectric radiometer is the most frequently used thermal detector at TKK. In a pyroelectric radiometer the rise of temperature of the absorber changes its surface charge or internal dipole-moment. [36, 37] This change can be converted to a measurable voltage. Because the voltage is proportional to the change in incident radiation, a mechanical chopper must be applied to chop the incident radiation in continuous-wave power measurements.

16

A common feature to all thermal detectors is that their power responsivity is, in principle, independent of the wavelength of the radiation. This is due to the fact that the measured signal of thermal detectors is directly proportional to the electromagnetic power of the radiation. Of course, the absorbance of the absorber of the detector is never perfect, and may have some dependence of wavelength. Lehman *et al*. have reported a 0.2-% uniformity for the responsivity of a pyroelectric radiometer, over the wavelength region of 0.8 – 1.8 μm. [38] This effect is, however, small as compared to the wavelength dependencies of quantum detectors. On the other hand, quantum detectors are typically much less noisy than thermal detectors. Also, thermal detectors follow the power changes in incident radiation much slower than quantum detectors.

The signal of a quantum detector is not proportional to the power of the incident radiation, but to the rate of incident photons per unit time. Since the energy of a photon is a function of the wavelength, the power responsivity of a quantum detector is also a function of the wavelength. Photodiodes are the most widely used quantum detectors. Also the work described in this thesis is strongly based on the use of photodiodes. Some of their main properties are described in the next section.

2.2.2 Properties of photodiodes

A photodiode is constructed of a junction of a *p*-type and an *n*-type semiconductor material. Often a non-doped layer is added between the *p* and *n*-doped layers. The purpose of this additional layer is to widen the depletion region of the diode. This structure is called *pin* photodiode. Physically speaking, a photodiode is identical to the diodes used as electrical components, except for the wider depletion region.

Several semiconductor materials can be used in photodiodes. The most commonly used material is silicon. Germanium [39], gallium arsenide phosphite [40] and indium gallium arsenide [20, 41, 42, Publication I] are also used. The choice of material is often based on its spectral properties. For example, silicon photodiodes are a fine choice for detectors in the visible region, long UV wavelengths, or short IR wavelengths. On the other hand, they do not produce any signal at telecommunication wavelengths. These matters are discussed in more detail in later sections. Also, matters like price, availability, size etc. can play a role in choosing the correct material.
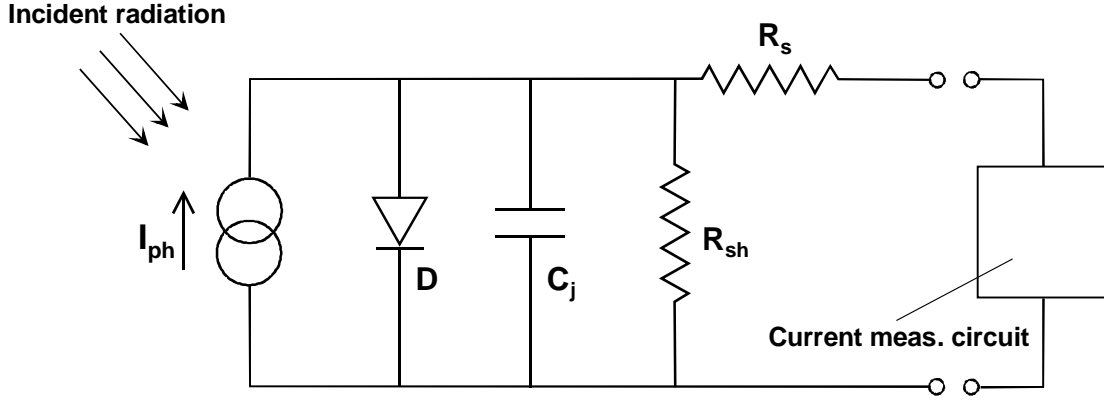
Figure 1. Equivalent circuit of the photodiode. I_{ph} **is photocurrent (proportional to incident radiation),** D **is a diode,** C_j **is the junction capacitance,** R_{sh} **is the shunt resistance and** R_s **is the series resistance.**

The equivalent circuit of the photodiode is shown in Figure 1. When a photon enters the depletion region, it generates an electron-hole pair. The internal potential difference between the layers draws the electrons and holes apart, thus creating a photocurrent I_{ph}. The direction of this current is to the reverse direction of the diode. In addition, a current to the forward direction is produced by the forward biased voltage V that appears over the diode. This is called dark current. The total current I_{tot} is

$$I_{tot} = I_{ph} - I_{dk}\left(e^{eV/kT} - 1\right),\qquad(1)$$

where the latter part represents the dark current. T in Eq. 1 is the absolute temperature, e is the elementary charge, k is Boltzmann's constant and I_{dk} is a current-constant.

Assuming that all incident photons enter the depletion region, that each photon generates one electron-hole pair, and using the energy of a photon, $E=hc/\lambda$, it is simple to derive the power responsivity R of an ideal photodiode as

$$R = \frac{I}{P} = \frac{e}{hc}\lambda,\qquad(2)$$

where P is the power of the incident radiation, h is Planck's constant, c is the speed of light and λ is wavelength. It can be seen that in the ideal case the responsivity is a linear function of the wavelength. Figure 2 shows the ideal and measured power responsivities of a silicon photodiode. The ideal responsivity obeys Eq. 2, until the energy of the photon, which is inversely proportional to the wavelength, has decreased below a threshold, called band gap energy E_g. This is the minimum energy that is required to generate an electron-hole pair. The wavelength corresponding to the photon energy E_g is called the cut-off wavelength. The most significant non-idealities of a silicon photodiode are the non-zero reflectance of the diode surface and the internal quantum efficiency that differs from unity. [12] Both these effects are

18

wavelength dependent. Figure 3 shows the modeled internal quantum efficiency and spectral reflectance of a silicon photodiode. [12]
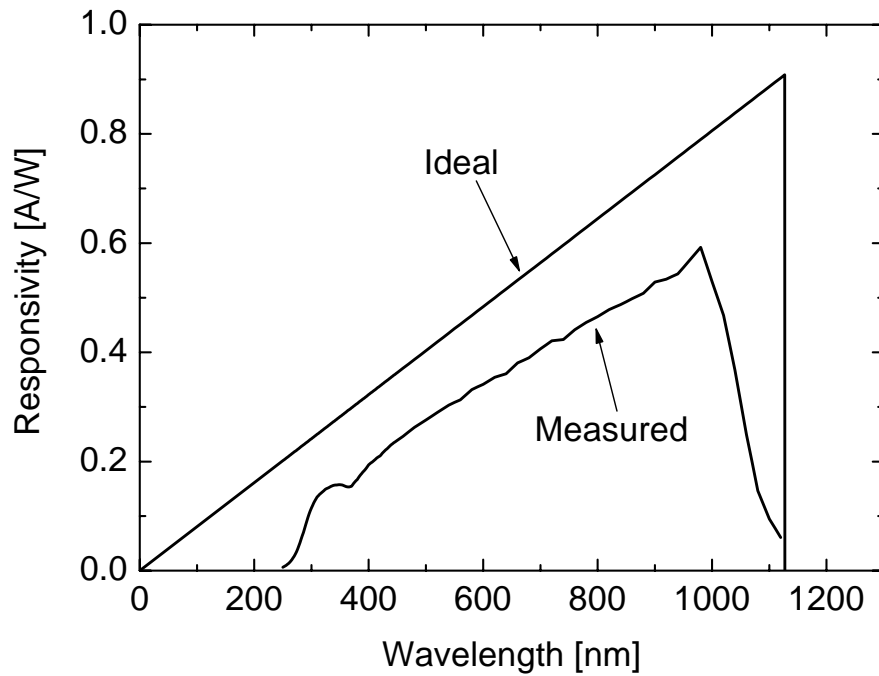

Figure 2. Ideal and measured [43] power responsivities of a Si photodiode. The band gap energy is set to 1.1 eV [44], corresponding to a cut-off wavelength of 1.13 μm.
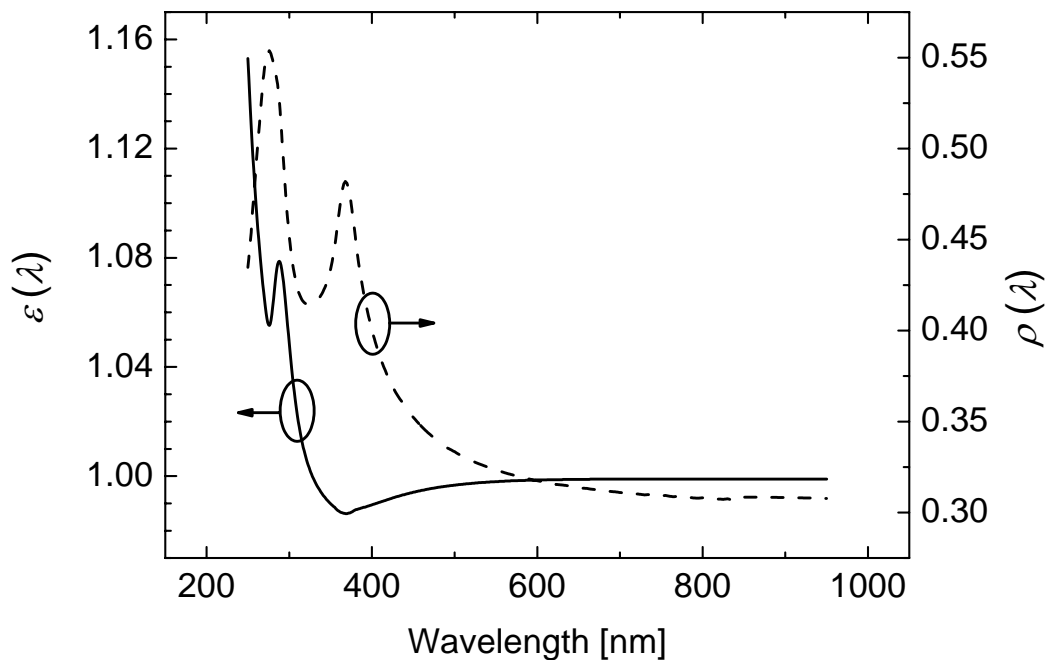
Figure 3. Internal quantum efficiency $\varepsilon(\lambda)$ **and spectral reflectance** $\rho(\lambda)$ **at normal incidence for a silicon photodiode.**

Typically the power responsivity of a photodiode is preferred to stay constant over a wide power range, i.e. the output current I_{tot} of the photodiode should be a linear function of the incident power. I_{ph} in Eq. 1 is directly proportional to the incident power, so in order to maintain the linearity of I_{tot} we must keep the dark current, and therefore voltage V, constant, preferably zero. This is achieved with correct choice of current measurement circuitry. In practical work, a transimpedance amplifier is used to convert the photocurrent into a voltage.

2.3 Scale realization and measurement standards at TKK

The cryogenic absolute radiometer is the primary standard of optical power at TKK. [6] Trap detectors, utilizing silicon photodiodes, are used as primary working standards. [45] Trap detector is a structure of several photodiodes, which are placed in such geometry, that the incident light is reflected several times from the surfaces of the photodiodes before exiting the trap. The photodiodes are connected electrically in parallel, so that the overall current signal of the trap is the sum of the signals of the individual photodiodes. Depending on the structure of the trap, the light may either pass through the trap, or return the same path that it entered the trap. These configurations are called the transmission trap and the reflection trap, respectively. The main benefit of the trap configuration is its significantly reduced reflectance, compared to a single photodiode. Typically the reduction of reflectance can be more than one decade. [49, 46] The reduced reflection of the detector is an important feature, when the detector is used as a building block of a filter radiometer. The low reflectance effectively reduces the effect of inter-reflections between the detector and

20

the band pass filter. [47] In addition, it should be noted that changes in the measurement environment, mainly humidity, may change the reflectance of the photodiode. [48] Hence, the change in humidity may cause a significant source of measurement uncertainty. [45] This uncertainty component is effectively minimized with the trap configuration. Figure 4 shows the geometry used in the reflection trap detectors at TKK. In this configuration the light undergoes two reflections from tilted photodiode surfaces, reflects back from the third photodiode, and returns the same path out of the trap. The total amount of reflections is thus five. Furthermore, the configuration of Figure 4 ensures that the responsivity of the trap is insensitive to polarization of the incident light.
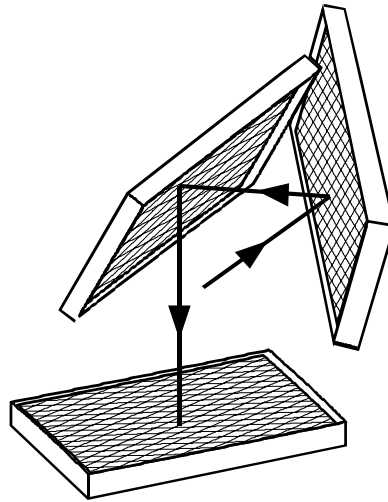
Figure 4. Geometry of the three photodiodes used in the reflection trap detectors at TKK. [49] The light undergoes five reflections from photodiode surfaces before exiting the trap. This configuration also makes the responsivity of the trap insensitive to polarization of incident light.

The responsivity of a silicon trap detector is measured at several laser wavelengths, after which the responsivity is interpolated, using physical models for spectral reflectance and internal quantum efficiency, to cover the wavelength region 260 – 950 nm. [12] At this wavelength range the trap detectors are used as the primary working standards at TKK. At longer wavelengths pyroelectric radiometers are used.

3 Fiber optic power measurements

3.1 Optical fibers

The material used in optical fibers is silica (SiO_2). The use of NIR radiation as the carrier wave in optical communication becomes self-evident when looking at the spectral attenuation of silica, shown in Figure 5. The most significant factors constituting to the attenuation are Rayleigh scattering and material absorption. Rayleigh scattering is a resultant of the fluctuations in density, and therefore fluctuations in refractive index, within silica. [50] The fluctuating refractive index scatters radiation to all directions. The effects of these phenomena are also plotted in Figure 5. Also the absorbance of certain impurities in silica causes attenuation. The most significant absorbing impurities are the OH$^-$ ions, that have a strong absorbance peak at 1.4 μm. This peak is sometimes referred to as "water peak." Nowadays, two wavelength windows are in common use. These windows are around the wavelengths 1.3 μm and 1.55 μm, where the attenuation of silica has local minima. Also a third band at 0.8 μm is used, but its significance in modern telecommunication is smaller than that of the other two. [13] In addition, the availability of optical amplifiers at the 1.55-μm window makes this wavelength band an attractive choice. The 1.55-μm band is further divided into C-band (1530 – 1565 nm), S-band (1460 – 1530 nm) and L-band (1565 – 1625 nm), where letters C, S and L stand for conventional, short and long, respectively. This division is based on the use of different optical amplifiers in different bands.
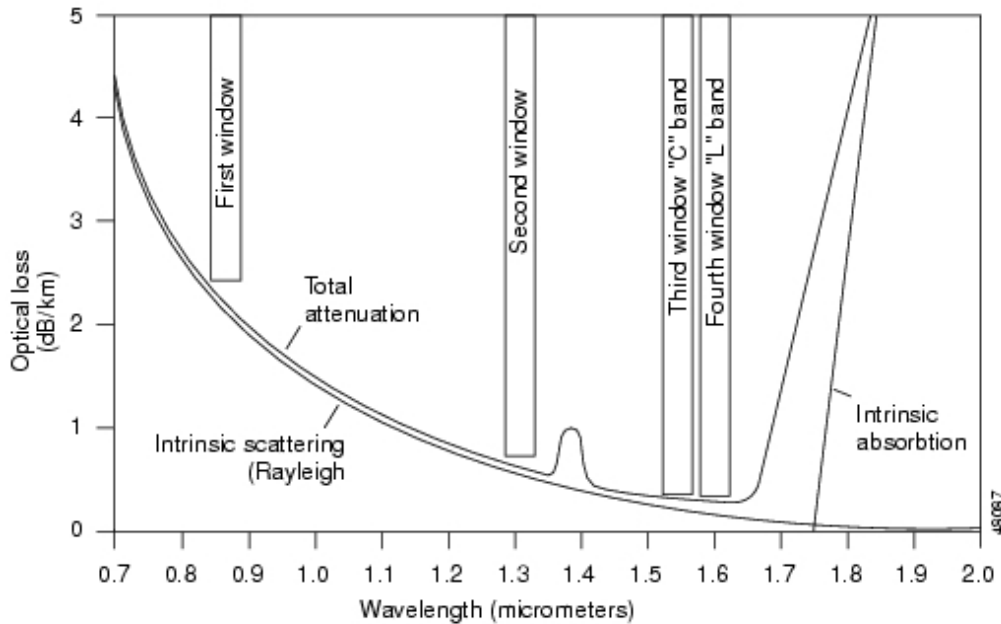

Figure 5. Spectral attenuation loss of silica. [51]

As suggested by Maxwell [52], light is an electromagnetic wave propagating in vacuum or in a medium. The electric and magnetic fields **E** and **H** of the wave must satisfy the wave equations

22

$$\nabla^2 \tilde{\mathbf{E}} + \frac{\omega^2 n^2(\omega)}{c^2} \tilde{\mathbf{E}} = 0 \quad \text{and} \tag{3}$$

$$\nabla^2 \tilde{\mathbf{H}} + \frac{\omega^2 n^2(\omega)}{c^2} \tilde{\mathbf{H}} = 0 \tag{4}$$

derived from the Maxwell's equations. In Eqs. 3 and 4, $\tilde{\mathbf{E}}$ and $\tilde{\mathbf{H}}$ are the Fourier transforms of $\mathbf{E}$ and $\mathbf{H}$, respectively, n is refractive index, and ω is angular frequency. The fields in both core and cladding must satisfy Eqs. 3 and 4. There are a finite number of solutions for the equations, and each solution constitutes a fiber mode. Different modes travel with different velocities within the fiber, causing pulse broadening. Therefore it is desirable to limit the possible number of modes to one. This can be done by adjusting the core radius a and/or the refractive indices, n_1 and n_2, of core and cladding. When these parameters satisfy the condition

$$\frac{2\pi}{\lambda} a \sqrt{n_1^2 - n_2^2} < 2.405, \tag{5}$$

only one mode will propagate in the fiber. Such fiber is called single-mode fiber. All fibers used in the work described in this thesis are single-mode fibers for the given wavelengths.

3.2 Optical amplifiers

The attenuation of a modern optical fiber is of the order of 0.2 dB/km. It is typically required that the signal must be amplified or regenerated when the power of the signal has attenuated 20 – 30 dB from the initial value at the transmitting end of the link. [13] Therefore it can be concluded that the signal must be amplified after every 100 – 150 km. Traditionally, the signal has been regenerated by transforming the optical signal into an electrical signal, amplifying the signal with an electrical amplifier, and finally transferring the signal back to optical form. The problem of this procedure is, that in a wavelength division multiplexing (WDM) system each channel must be amplified separately. The number of receivers (detectors and electrical circuitry), amplifiers and transmitters (lasers and encoding circuitry) needed equals to the number of channels being transmitted. The number of channels in DWDM (dense WDM) systems may be around 100.

Introduction of the erbium doped fiber amplifier (EDFA) in 1987 [53] improved the situation considerably. EDFA is an all-optical amplifier that utilizes stimulated emission of the rare-earth element erbium. In practice, the device contains a fiber doped with erbium impurities. The gain profile of erbium enables light to be amplified over the wavelength region 1525 – 1570 nm. The population inversion within the erbium atoms is maintained by use of pump lasers, typically at 980- or 1480-nm wavelength. The transmitting power of EDFA can be in the 1-W range. The fact that the maximum of the gain profile of erbium coincides with the minimum of the spectral attenuation loss of silica, shown in Figure 5, has made the 1.55-µm wavelength window extremely popular. Finally it should be noted that due to its wide

gain profile, EDFA is able to amplify all the channels of a WDM link simultaneously. This significantly simplifies the structure of the link. Also, unlike regenerators, EDFA is insensitive to the bit rate or signal format. [13]

EDFA is the most widely used optical amplifier, and it is meant for use at the C-band. Slightly modifying the doping or the length of the erbium doped fiber within the device EDFA can also be used at the L-band. This, on the other hand, also increases the amplification at the C-band. Typically C-band- and L-band-EDFA's are separate devices and the signal is divided into C-band and L-band parts with a demultiplexer before amplification. Raman amplifiers are optical amplifiers utilizing the non-linear effect stimulated Raman scattering, in which signal energy is transferred from shorter wavelengths to longer wavelengths. When applied in optical amplification, this effect enables signals at the S-band to be amplified. Semiconductor optical amplifiers (SOA's) have a construction quite similar to that of semiconductor laser – without optical feedback, of course. SOA's are able to amplify signals both at 1.3-μm and 1.55-μm bands. At the 1.55-μm band EDFA's are preferred over SOA's, mainly because of the severe crosstalk caused by SOA's in WDM systems. Also, EDFA reaches higher gains and output powers, and its coupling losses and polarization-dependent losses are lower. [13]

In fiber optic power measurements, an EDFA can be used to produce fiber optic power at the level of hundreds of milliwatts. The use of an EDFA in fiber optic metrology is further discussed in later sections and in Publication II.

3.3 Detectors for fiber optic power measurements

3.3.1 Measurement geometry

Measurement of fiber optic power has certain special characteristics as compared to non-fiber based optical power measurements. The main problem arises from the difference in measurement geometries between fiber measurements and measurements with free-space laser beams. [15, 16, 19, 20, 21, 35, Publication I] The absolute power calibration of a fiber optic power meter (FOPM) is often performed with a collimated laser beam, while the actual measurements with the detector are performed with a fiber. Figure 6 demonstrates this difference. Figure 6a shows the case in which the light spreads from the end of an optical fiber into a wide solid angle Ω, while Figure 6b depicts the case of a collimated laser beam. The size of the illuminated area A is typically different in these two cases. If we assume the optical powers of Figure 6a and Figure 6b to be equal, the responses by the photodetector are equal only if the power responsivity of the detector has no angular or spatial dependence. If such dependence exists, as is the case for most practical detectors, a systematic calibration error is introduced due to the change in geometry. In principle there are two ways to reduce this effect. One is to use a detector with minimal spatial and angular non-uniformities as FOPM. The other way is to characterize these non-uniformities and calculate corrections to compensate for them.
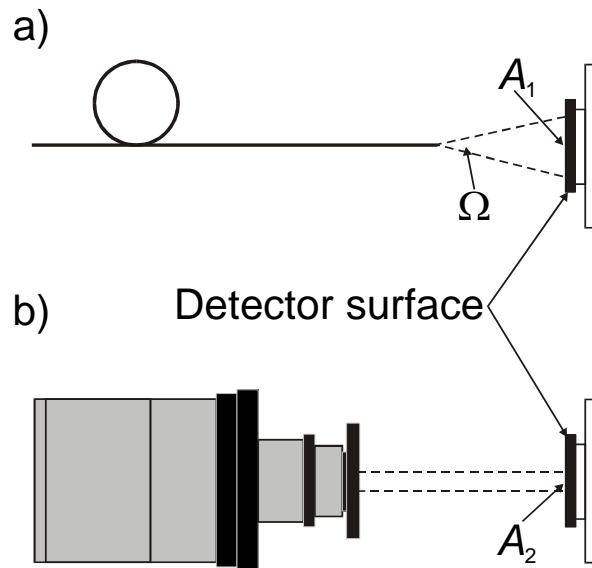
Figure 6. Difference in measurement geometry between a) fiber measurements and b) measurements with collimated beam.

3.3.2 Photodiodes for NIR wavelengths

When choosing a photodiode for measurements at NIR region, two semiconductor materials are in wide use – germanium (Ge) and indium gallium arsenide (InGaAs). Figure 7 shows the measured spectral responsivities of InGaAs and Ge photodiodes. Also the responsivity of the silicon (Si) photodiode, depicted in Figure 2, is given for reference. A typical value for the E_g of Ge, at room temperature, is 0.66 eV. [54] E_g of InGaAs varies as a function of the amount of In doping. [55, 56] Values between 0.36 and 1.43 eV are possible. [56]
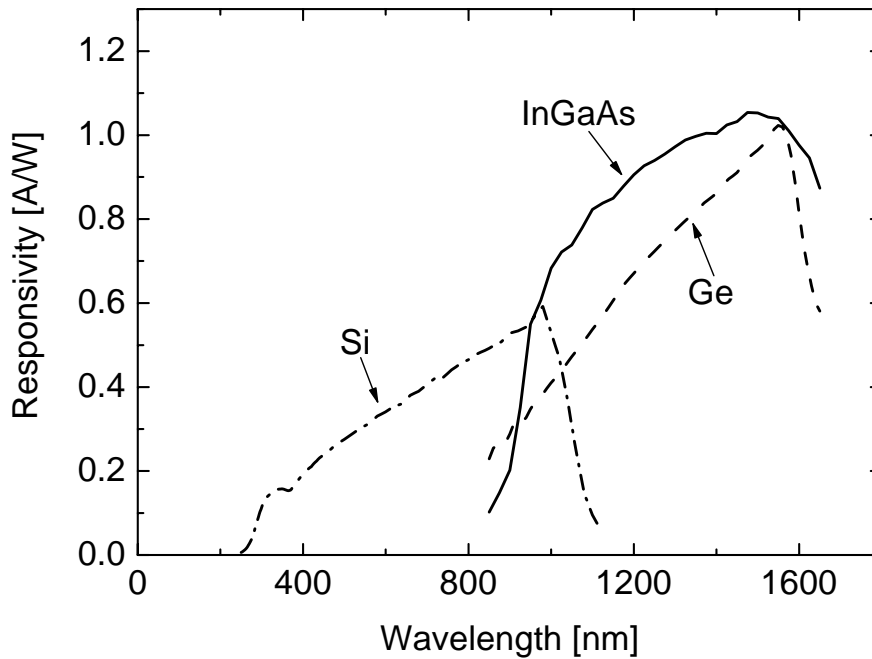
Figure 7. Measured spectral responsivitites of Si, InGaAs and Ge photodiodes.

The main problem with Ge photodiodes is their high level of noise, which limits the dynamic range of their use. The high noise level is primarily caused by the low shunt resistance of Ge photodiodes. [41] It can be seen in Figure 1 that decreasing shunt resistance will result in more photocurrent flowing through it. If the shunt resistance decreases so much that it is of the order of magnitude of the input resistance of the current measurement circuit, a significant part of the current will be lost, in the measurement point of view. Also, this will result in a larger voltage V to appear over the diode, which leads to a larger dark current. Dark current, on the other hand, is noisy by nature. This can be verified, for example, by looking at Eq. 1, in which the dark current has an exponential dependence on temperature. In addition, at the 1550-nm wavelength window, the responsivity of Ge photodiodes is quite sensitive to temperature. At 1550 nm, the temperature coefficient of the responsivity is close to zero, but then it increases rapidly as a function of the wavelength, being $\sim 10^{-2}$ °C^{-1} at 1600 nm. [41] The advantage of Ge photodiodes over InGaAs photodiodes is that Ge diodes are available in large sizes at reasonable price. [57] This is a desired feature in radiometric applications.

The radiometric properties of InGaAs photodiodes are superior as compared to those of Ge diodes. The shunt resistance of InGaAs diodes is higher, making the dark current smaller. [20, 42] Fox [41] has reported of InGaAs photodiodes with a 10-pA dark current, which is an order of magnitude smaller than that of the best commercially available Ge diodes of the same size (100 mm^2). The temperature dependence of the power responsivity of InGaAs photodiodes is negligible at telecommunication wavelengths. Boivin [20] and Stock [42] have reported values of

26

$2 - 4 \times 10^{-4}$ °C^{-1}. One specific feature of InGaAs photodiodes is the sharp drop in responsivity at shorter wavelengths, as seen in Figure 7. This is caused by absorbance of the InP layer, which is grown on the surface of InGaAs to protect it from aging effects and environmental hazards. [42]

3.3.3 Integrating sphere

In general, the power responsivity of any real detector is more or less dependent on the geometry of the measurement setup. By geometry we mean the spatial and angular distribution of the incident radiation. This issue is especially significant in fiber optic measurements, as discussed in section 3.3.1.

Integrating sphere radiometer is a detector whose power responsivity has very small dependence on the geometry and alignment of incident radiation, i.e. it is said to spatially (and angularly) integrate the incoming power. Figure 8 shows a schematic picture of a simple sphere radiometer. The sphere itself is a spherical cavity whose walls are made of – or coated with – a material with diffuse reflectance near unity over a wide wavelength range. The sphere of Figure 8 has one entrance port and one exit port. A photodetector is attached on the exit port. It can be shown that the signal, given by the detector, is proportional only to the total power of incident radiation – spatial or angular distribution of incident radiation has very little effect on the signal. [58]
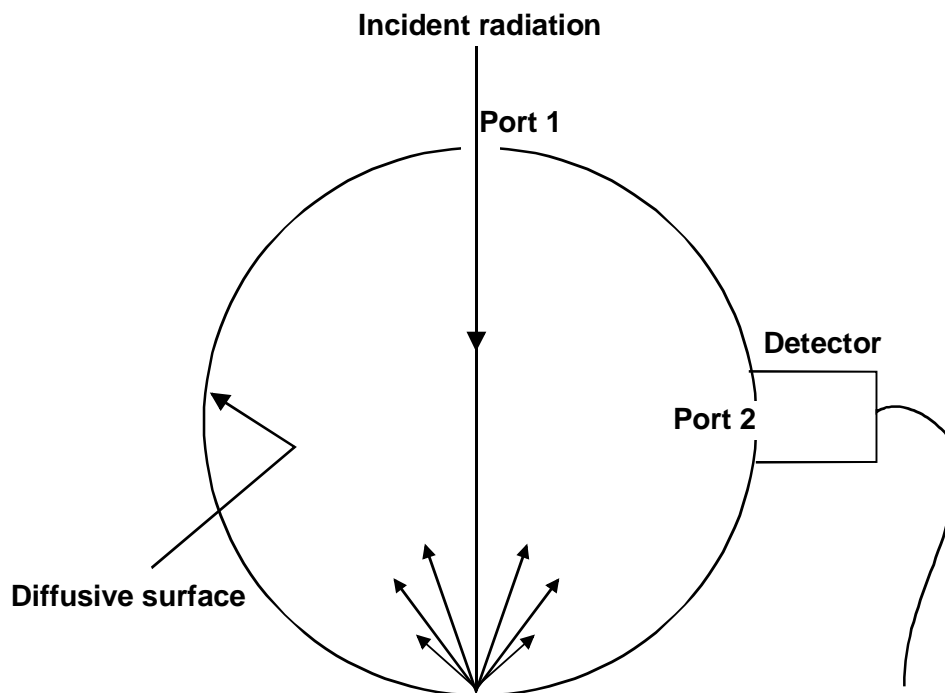

Figure 8. Structure of an integrating sphere radiometer.

In order to maximize the diffuse reflectance of the sphere wall, a suitable material must be chosen for the inner wall of the cavity. Available materials include barium sulfate, gold, OP.DI.MA, Spectraflect™, Duraflect™, Spectralon® and Infragold™.

OP.DI.MA is a commercial material developed by Gigahertz-Optik GmbH. Spectraflect, Duraflect, Spectralon and Infragold are commercial materials developed by Labsphere Inc. In the NIR region, gold, OP.DI.MA, Spectralon and Infragold are suitable choices; they all are specified of having a diffuse reflectance greater than 95 % at this wavelength region. [59, 60]

3.4 Measurements of fiber optic power at TKK

The scale of fiber optic power can be realized by constructing and characterizing a FOPM that has a connector for fiber optic cable and whose power responsivity can be accurately measured against a known standard for optical power. Several types of trap detectors, integrating sphere detectors, thermopile detectors or simple plain photodiodes can be used as a FOPM. [15, 16, 19, 20, 21, Publication I, Publication II]

Two types of reference detectors have been studied at TKK. One type utilizes plain photodiodes, the other type consists of an integrating sphere and a photodiode. All FOPM's have been characterized for 1310-nm and 1550-nm wavelength windows. The precise wavelengths used in the measurements were 1308.4 nm and 1552.5 nm, if not stated otherwise.

3.4.1 Detectors utilizing plain InGaAs photodiodes

Figure 9 shows the construction of the fiber optic detectors utilizing plain InGaAs photodiodes. The active area of the photodiode is circular with 5-mm diameter. Photodiodes are fitted into aluminum cases equipped with adapters for fiber optic cable and output connectors for the current signal of the photodiode. Figure 10 shows photographs of an idividual photodiode and the detectors with plain photodiodes.
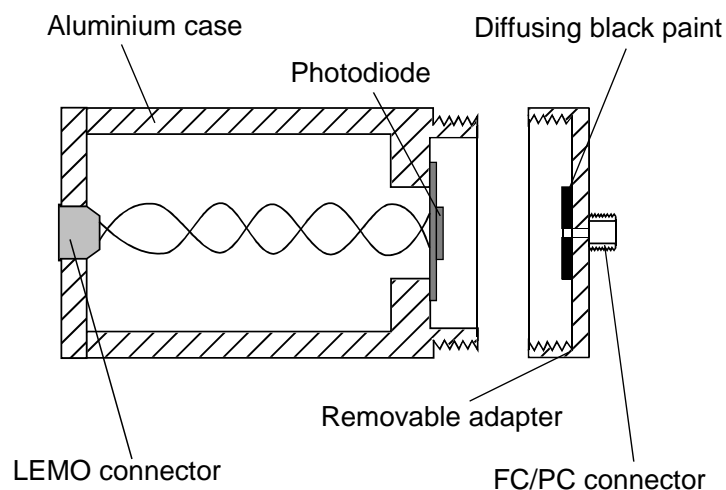

Figure 9. Structure of detectors utilizing plain InGaAs photodiodes. [Publication I]

28

Figure 10. On the left: close-up of the InGaAs photodiode GAP5007 (Germanium Power Devices Inc.). On the right: assembled detectors with plain photodiodes with and without the fiber adapter.

On the inside surface of the adapter there is an area of diffusing black paint to reduce inter-reflections between the diode and the adapter. Two of these detectors were built and studied. They will later on be referred to as FOPM-1 and FOPM-2.

To compensate for the calibration errors due to the geometrical issues, discussed in section 3.3.1, the spatial and angular dependences of the responsivity were measured for both photodiodes. Figure 11 and Figure 12 show the results.
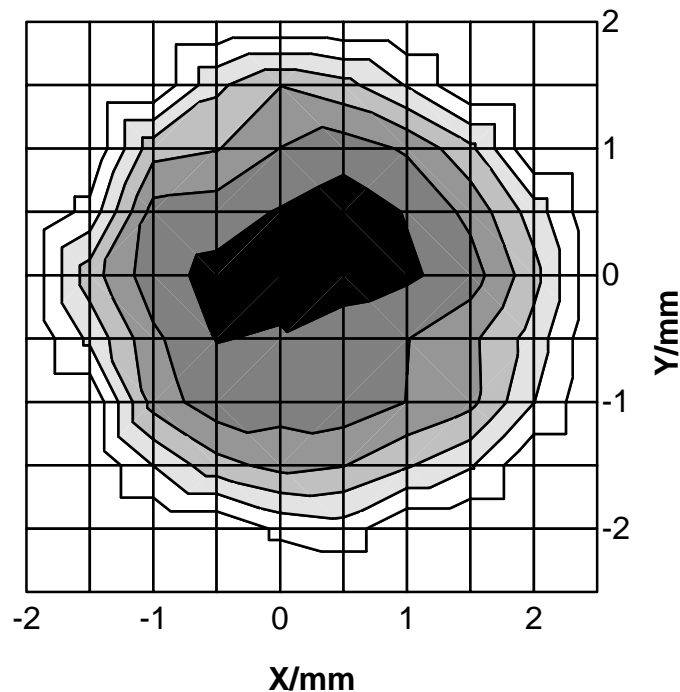

Figure 11. Measured spatial non-uniformity of the power responsivity of FOPM-1 at 1310-nm wavelength. Each contour line indicates a

drop of 0.2 % in the responsivity. Data have been normalized to the responsivity at the center.
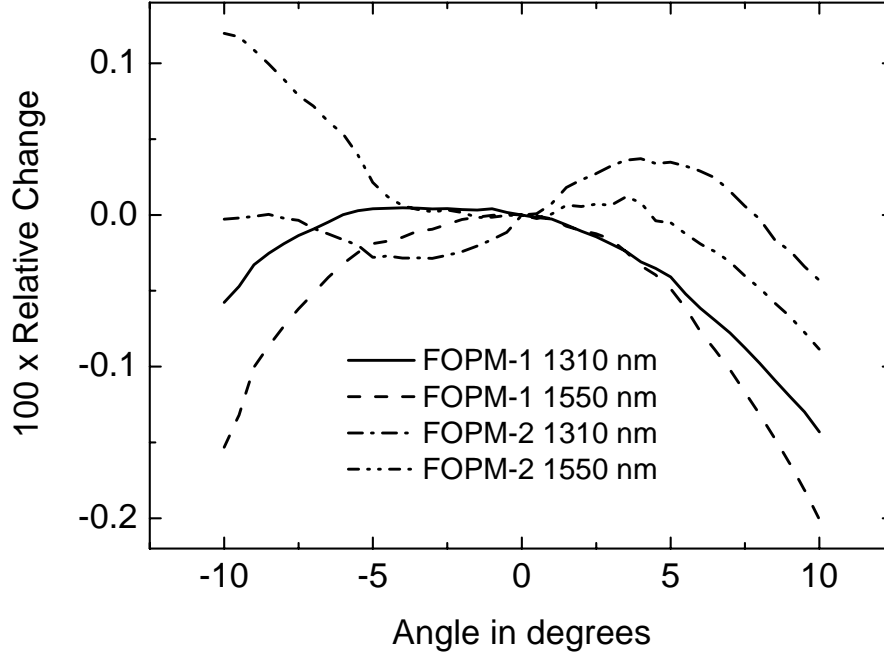

Figure 12. Measured angular non-uniformity of the power responsivity of the plain photodiodes. The values are given as the relative change from the responsivity at zero-angle. The difference in curve shapes between the detectors can be explained by different anti-reflection coatings used in the photodiodes.

It has been shown in Publication I, that the correction to compensate for the measurement geometry varied between -0.35×10^{-4} and 1.2×10^{-4}. The correction C due to angular non-uniformity was calculated as

$$
C = \frac{\displaystyle\int_{\theta_1}^{\theta_2} P_{ang}(\theta)\, d\theta}{\displaystyle\int_{\theta_1}^{\theta_2} R_{ang}(\theta)\, P_{ang}(\theta)\, d\theta} - 1,
\tag{6}
$$

where R_{ang} is the measured angular responsivity, P_{ang} is the angular power distribution, θ is the directional angle, and θ_1 and θ_2 limit the angular interval in which a significant part of the emitted power exists. Calculation of the correction for the spatial non-uniformity was impossible because of the inadequate resolution of the spatial non-uniformity measurement. Instead, the effect of spatial non-uniformity was included in the uncertainty budget.

The reflectances of the photodiodes were measured for both wavelengths in order to estimate the magnitude of the rise in response due to inter-reflections between the diode surface and the fiber adapter. The reflections varied between 1.5 and 8.8 %. The rise in response due to inter-reflections was estimated to be 2.3×10^{-3} at maximum.

The absolute responsivity measurements for FOPM-1 and FOPM-2 were performed using a collimated laser beam. The reference detector in the measurements was a pyroelectric radiometer, traceable to the cryogenic absolute radiometer of TKK. FOPM-1 and FOPM-2 can be used for measurements with power levels up to 7 mW. The non-linearity within this power range was measured to be better than 10^{-3}. The uncertainty of the power responsivity is 0.9 % (k=2) for both detectors and wavelengths.

3.4.2 Integrating sphere detector

The structure of the integrating sphere detector is depicted in Figure 13. The sphere was custom made for this project and it was manufactured by Labsphere Inc. The inner diameter of the sphere is 50.8 mm and it is entirely constructed of Spectralon. It has two entrance ports, one of which (port 1) has mountings for a fiber adapter. The other entrance port (port 2) can be covered with a Spectralon plug. The exit port of the sphere has an InGaAs photodiode attached to it.
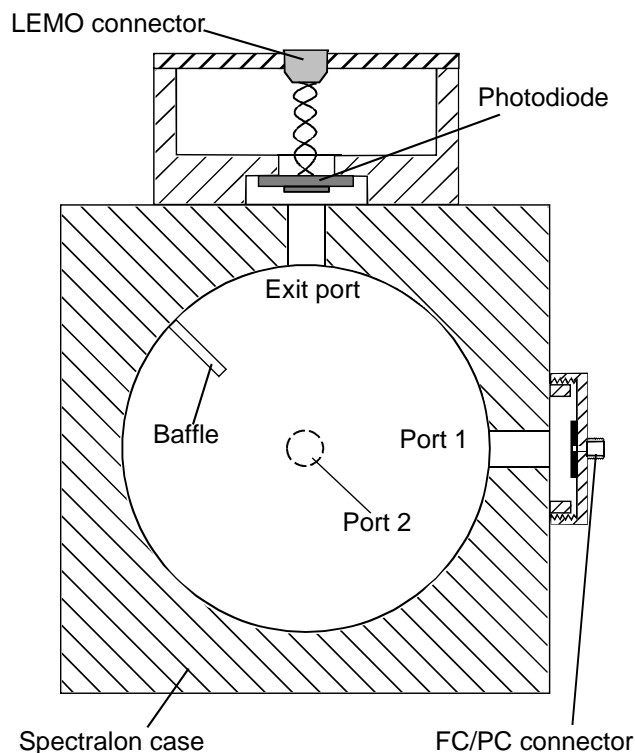

Figure 13. The structure of the integrating sphere detector. [Publication I]

The throughput of the sphere is quite low, ~0.7 %. Therefore the sphere detector is well suited for measurements at relatively high power levels. Theoretically, it should be possible to use the sphere at power levels up to 1 W.

Integrating spheres typically have one entrance port only, which can either be open for collimated beams, or covered with a fiber optic connector, as shown in Figure 8. Theoretically, this has an effect on the throughput of the sphere and thus the responsivity. This effect, if significant, may introduce a systematic calibration error. This is due to the difference in measurement geometry between absolute power responsivity calibration, where the fiber connector is removed, and fiber measurements in which the connector is attached. To study this effect, we measured the responsivity of the sphere detector via port 2 while port 1 was either open or covered with the fiber adapter. The relative difference in responsivity was less than 10^{-3}. The effect is negligible as compared with the desired uncertainties.

The correction factor due to measurement geometry was found negligible for the integrating sphere detector, as seen in Publication I. The absolute responsivity measurements were performed using a collimated laser beam via port 1, against a pyroelectric radiometer. The fiber adapter was removed during the measurements. The uncertainty of the power responsivity is 0.8 % (k=2) for measurements at 1-mW level and 1.3 % (k=2) at ~100-mW level. [Publication I, Publication II, 61]

Because the sphere detector is to be used also at high power levels, its aging properties had to be examined. The aging can be accounted for by estimating the total exposure of the detector to high power levels during a certain period, and subsequently by exposing the detector to the highest measurable power for this estimated time. The power responsivity of the detector is measured before and after the exposure. Possible aging noted is accounted for in the uncertainty budget. Alternatively, the calibration interval of the detector can be kept sufficiently short so that the aging effect can be neglected.
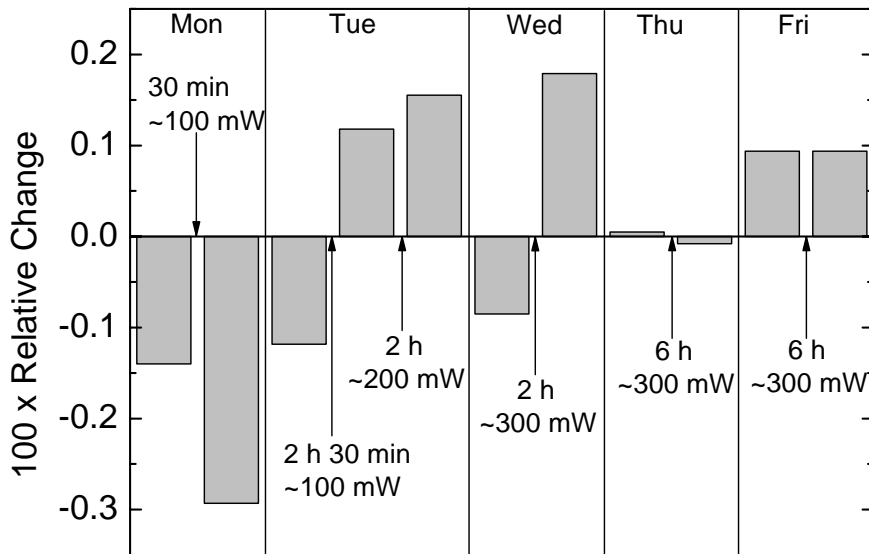
Figure 14. The results of the aging test. The bars denote the results of the power responsivity measurements, given as the relative change from the average of all measurements. The labels give the optical power and time of exposure used during the aging periods.

The aging properties of the sphere detector were examined by exposing it for high optical power (100 – 300 mW) for total of 20 hours. An EDFA was used to produce the high power levels. Figure 14 shows the schedule of the aging, with the measured responsivities during the process. The test was performed during a five-day period. During each day the sphere was aged 2-3 times. The responsivity of the sphere detector, with respect to FOPM-1, was measured between the aging periods, as well as in the beginning and in the end of each day. The responsivity measurements were performed at ~1-mW level without the EDFA. During this test the power responsivity of the detector remained the same within a standard deviation of 0.15 %.

In a recent study, conducted at TKK, Lamminpää *et al.* [62] measured the non-linearity of the responsivity of the sphere detector. Figure 15 shows the results.
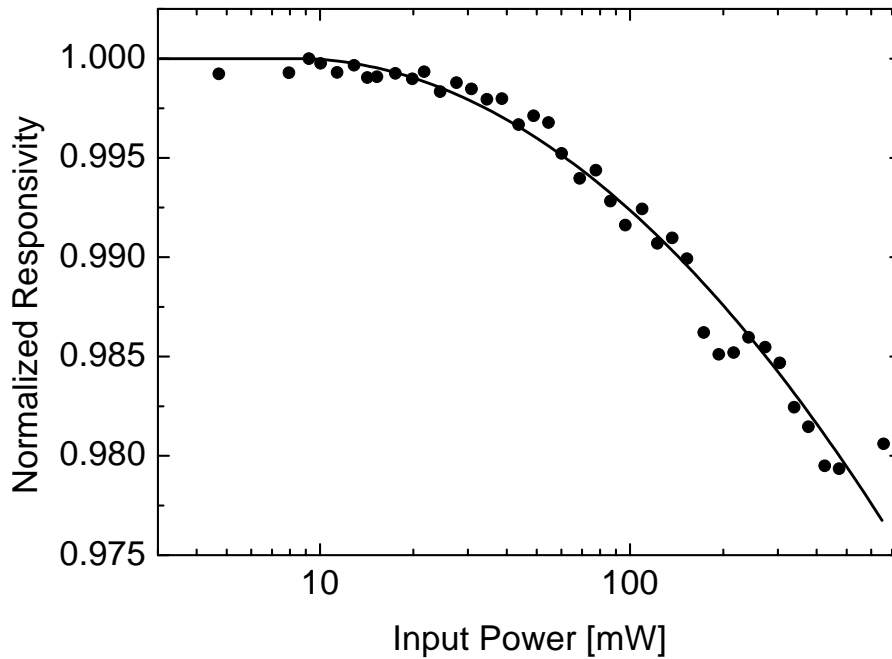
Figure 15. Measured non-linearity of the power responsivity of the sphere detector. The solid line represents a second order polynomial fitted to the measured data.

3.5 Comparison measurements between TKK, SP and DFM

In order to verify the reliability of the scale of fiber optic power, TKK performed a trilateral comparison of scales with Swedish National Testing and Research Institute (SP) and Danish Fundamental Metrology (DFM). The scales were compared at 1550-nm wavelength window with several power levels ranging from 1 mW to 200 mW.

Different types of reference detectors were used in the comparison. TKK used FOPM-1 and the integrating sphere detector described above. SP used a thermopile detector, while DFM had two sphere detectors, equipped with Ge photodiodes.

Figure 16 shows the results of the high-power comparison. The outcome of the comparison was successful. The results of all the laboratories were within measurement uncertainties of the reference value of the comparison. The stated measurement uncertainties were 1.3 %, 2.9 % and 1.3 % for TKK, SP and DFM, respectively ($k=2$).
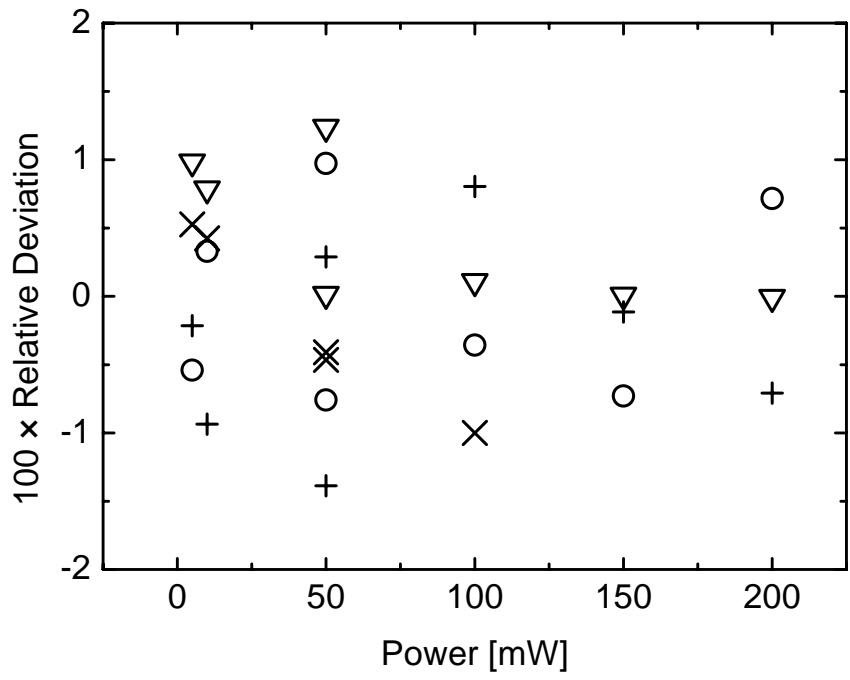
Figure 16. Results of the trilateral comparison of high fiber optic power scales between TKK, SP and DFM. +, SP; O, TKK integrating sphere; X, DFM large sphere; ∇, DFM small sphere.

4 Broadband ultraviolet measurements

4.1 Spectrally weighted UV measurements

UV radiation is all around us. It exists in the nature as a part of the solar spectrum. It can also be produced artificially. Numerous kinds of radiation sources, both coherent and non-coherent, are used to produce UV radiation for the needs of science and technology.

Measuring UV radiation can be a complicated task. To begin with, it should be determined what property is of interest. The same radiation that makes the human skin red, does not necessarily cause skin cancer, nor does it do the desired effect on the photoresist used in UV litography. All the effects mentioned above are strongly dependent on the spectrum of the UV radiation. Mathematically speaking, the quantity S of interest can be expressed as

$$S = \int_0^\infty s_{act}(\lambda)E(\lambda)d\lambda , \tag{7}$$

where $s_{act}(\lambda)$ is called the actinic function and $E(\lambda)$ is the spectral irradiance. The actinic function $s_{act}(\lambda)$ is a measure of how different wavelengths contribute to the effect in question.

4.2 Broadband UV detectors

A broadband detector is a detector that senses radiation over a wide wavelength band. Typically the band can be tens or hundreds of nanometers wide. In many cases the spectral responsivity $s(\lambda)$ of the detector is made to follow some specific actinic function $s_{act}(\lambda)$. In theory, if the shape of $s(\lambda)$ was an exact match of the ideal $s_{act},(\lambda)$, the signal of the detector would be directly proportional to the effect in question.

Different kinds of broadband UV detectors exist with various shapes of $s(\lambda)$. Erythema meters measure the effect of skin reddening. Their $s(\lambda)$ is made to follow the erythema action spectrum. [31] UVA and UVB meters are examples of detectors whose $s(\lambda)$ have a rectangular shape. These detectors measure the total amount of UVA (315 – 400 nm) or UVB (280 – 315 nm) radiation with no additional spectral weighting.

4.3 Calibration methods

Calibration of broadband detectors has proven to be anything but straightforward. Several international comparison measurements have been organized. The discrepancies between the results of the participants have exceeded the stated measurement uncertainties in many comparisons. [34] In order to have reliable, consistent measurement results, one must notice that the measured responsivity of the detector is strongly source dependent. If the detector is used to measure other sources

whose spectra differ from the spectrum of the source used in the calibration, severe discrepancies may occur. [32] Since the late 1990's several workers, like Xu [32, 33, 63], Larason [30, 64, 66] and Coleman [65], have developed calibration methods for the special needs of broadband calibrations. In practice, three methods are in wide use.

4.3.1 Line source calibration

In the simplest method, the responsivity of the detector is measured at a single wavelength. The monochromatic radiation can be produced by selecting a suitable emission line of a gas discharge lamp. For example, mercury lamps can be used to obtain intense emission lines at the UV range. This method can be recommended only for detectors with a simple, well defined $s(\lambda)$. It is also a good method to monitor the stability of the responsivity. Of all the three methods, line source calibration is the fastest to perform, and therefore the cheapest for the customer.

4.3.2 Spectroradiometric calibration

In this method, a spectroradiometer is used to measure the spectral irradiance of the radiation source. The detector, which is to be calibrated, is positioned at the same location where the spectral irradiance was measured and its signal is recorded. The responsivity R of the detector is obtained as

$$R = \frac{I}{\int\limits_{0}^{\infty} s_{act}(\lambda)E(\lambda)d\lambda}, \tag{8}$$

where I is the current signal of the detector.

4.3.3 Calibration using the measured $s(\lambda)$

In this method, the spectral irradiance responsivity $s(\lambda)$ of the detector is measured. The measurement can be done with a monochromator-based method [65, 66, Publication III] or with a tunable laser. [66] Once the $s(\lambda)$ is known, the responsivity of the detector can be calculated for any radiation source as

$$R = \frac{\int\limits_{0}^{\infty} s(\lambda)E(\lambda)d\lambda}{\int\limits_{0}^{\infty} s_{act}(\lambda)E(\lambda)d\lambda}. \tag{9}$$

The spectral irradiance $E(\lambda)$ in Eq. 9 is present both in the numerator and the denominator. Hence the absolute $E(\lambda)$ is not needed, only the relative shape of $E(\lambda)$ is required. This, on the other hand, means that $E(\lambda)$ does not need to be measured.

Instead it can be obtained from literature, or some suitable earlier measurement data can be used in the analysis.

We will hereafter call these three calibration methods *line source method* (LS), *spectroradiometric method* (SR) and *spectral irradiance responsivity method* (SIR).

4.4   Setup for measuring $s(\lambda)$

A monochromator-based measurement setup for measuring $s(\lambda)$ has been developed at TKK. [Publication III] Figure 17 shows a schematic picture of the setup.
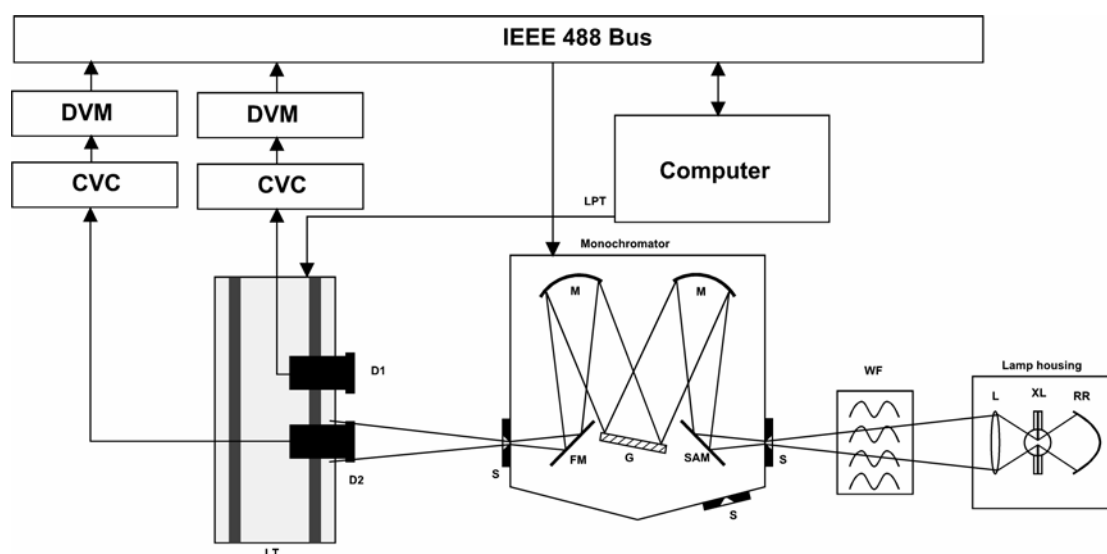

Figure 17. The setup used in the measurement of s(λ). Abbreviations: XL Xenon lamp; RR rear reflector; L lens; WF water filter; S slit; SAM swing away mirror; M collimating/focusing mirror; G grating; FM flat mirror; D1 and D2 detectors; LT linear translator; CVC current-to-voltage converter (transimpedance amplifier); DVM digital voltmeter; LPT parallel port of PC.

A 450-W xenon arc lamp is used as the radiation source. A single grating monochromator is used for spectral selection. The spectral irradiance responsivity is measured against a known reference detector. The measurements are performed in over-filled mode in the diverging beam.

Two UV enhanced silicon photodiodes are used as the reference detectors. The photodiodes have been fitted into aluminun cases and they have been equipped with precision apertures. The apertures are circular with diameters of 8 mm and 13 mm. These two detectors are labeled UVPD-8 and UVPD-13, respectively. The $s(\lambda)$'s of the photodiodes have been measured against a pyroelectric radiometer, traceable to the cryogenic absolute radiometer of TKK.

38

4.5 Comparing methods

Publication III demonstrates a successful comparison of SR and SIR methods. A commercial UVA detector (Figure 18) was used in the measurements.
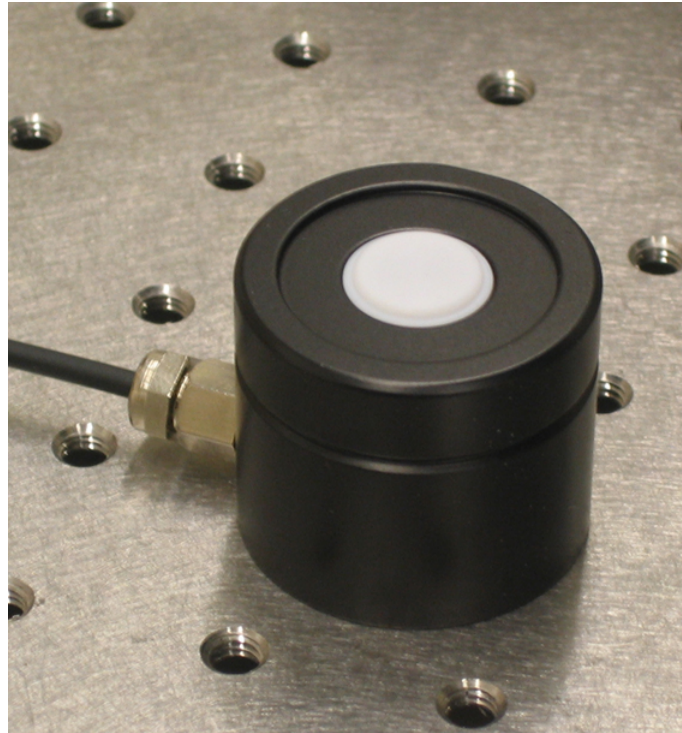
Figure 18. UVA detector UV-3701, Gigahertz-Optik GmbH.

Figure 19 shows the measured $s(\lambda)$ of the UVA detector. The ideal $s_{act}(\lambda)$ for a UVA meter is also shown. The UVA irradiance responsivity of the detector was calculated using Eq. 9 for two UV tubes. The calibration was repeated using the SR method. The difference in the results of different calibration methods was 1.2 %. The uncertainty of the comparison was 3.7 % (k=2).
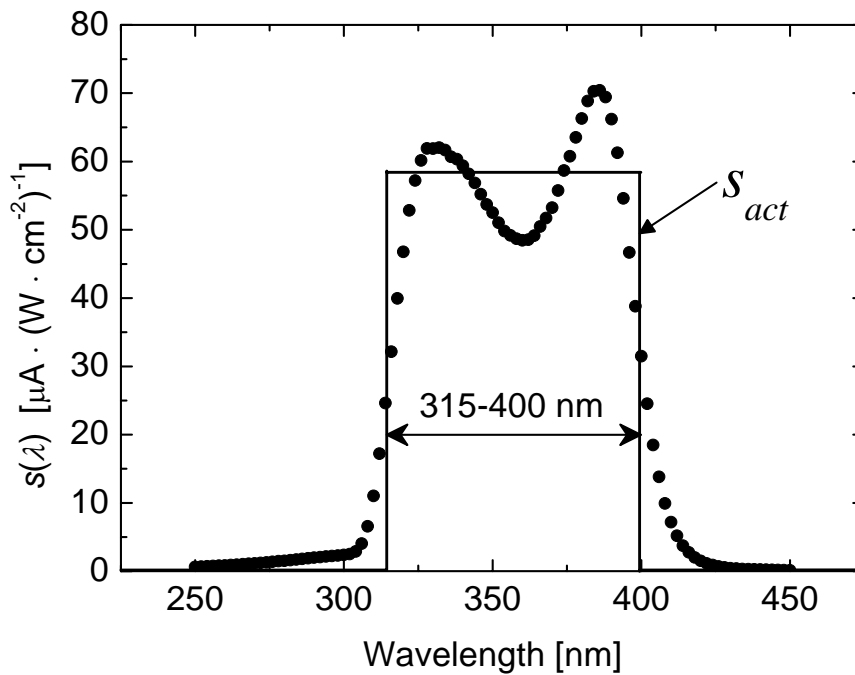
Figure 19. The measured $s(\lambda)$ of the UVA detector. Also the ideal $s_{act}(\lambda)$ of a UVA detector is shown.

In the measurements with the SR method, the geometry of the measurement setup had to be taken into account. In the ideal case, the diffuser of a broadband detector should receive radiation equally from all directions. When this kind of diffuser is over-filled with incident radiation, its angular response should follow the cosinusoidal shape. In practise, the angular response of the diffuser may differ considerably from the ideal shape. This problem is emphasized with large angles, with respect to the normal of the diffuser plane. [67, 68] The angular responses of the diffusers of the UVA meter and the measuring head of the spectroradiometer were measured. Figure 20 shows the results.

Figure 20. The measured angular responses of UVA detector and spectroradiometer.

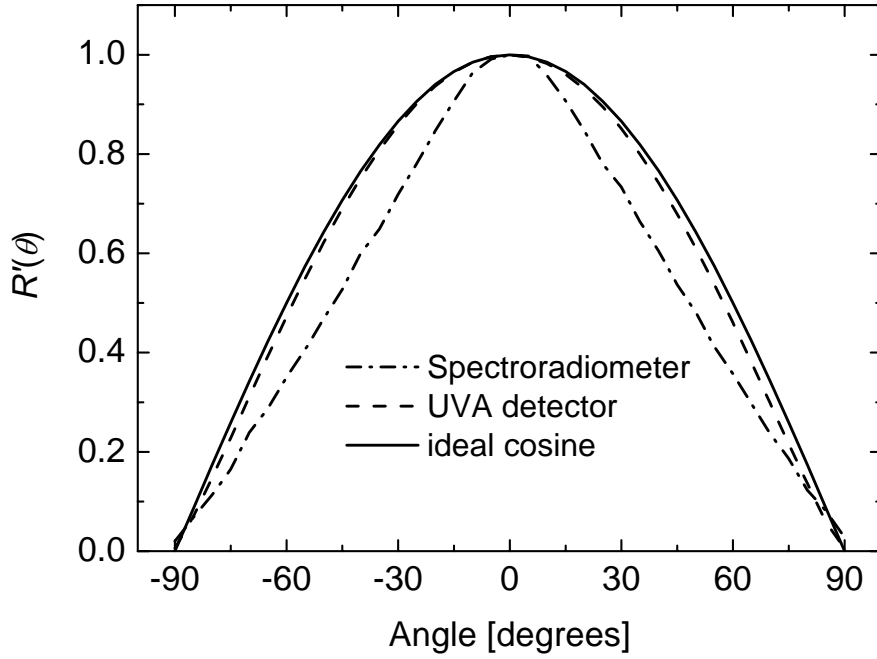A correction factor was derived [Publication III] to compensate for the systematic error due to measurement geometry;

$$C_{ang} = \frac{\int\limits_{-\theta_0}^{\theta_0} \cos^2 \theta \, d\theta}{\int\limits_{-\theta_0}^{\theta_0} R^{'}(\theta) \cdot \cos \theta \, d\theta} \, , \tag{10}$$

where $R'(\theta)$ is the measured angular response of the detector and θ is the angle with respect to the normal of the detector surface. In the measurements with the SIR method these corrections can be omitted, since the viewing angle of the detectors is relatively small in those measurements.

4.6 Inter-comparisons utilizing measured $s(\lambda)$

As stated above, calibrations of broadband detectors can be challenging. Therefore it is hardly a surprise that comparing the performance of different calibration facilities can also be tricky enough. Since the result of the calibration is dependent both on the radiation source and the measurement geometry used, the results of different calibration laboratories vary by definition. Therefore a direct comparison of the results is impossible. To overcome this problem, it is possible to instruct all the participants of the comparison to use same kinds of radiation sources and

41

measurement geometries, even a common source could be used in the comparison. [69]

In Publication IV we have introduced a novel method to be used in inter-comparisons of broadband detectors. The method relies on the use of the SIR method, described above. The principle of the comparison is that each laboratory will perform the calibration with the methods, sources, and setups that are used in their regular work. It is up to the pilot laboratory to assign individual reference values for each participant, against which the participants' results are compared. In order to do this, the pilot laboratory uses the earlier measured $s(\lambda)$ and the angular response of the detector, combined with the spectrum of the radiation source used by the participant, along with the information of the geometry of the participant's measurement setup. Having all these data, the pilot is able to calculate the responsivity to the source used by the participant with Eq. 9. The geometrical correction, if needed, is calculated with Eq. 10.

To validate the method, TKK organized a pilot comparison with four other European institutes. The participants were the Radiation and Nuclear Safety Authority (STUK, Finland), Photobiology Unit of the University of Dundee (United Kingdom), Medical Physics Laboratory of Guy's & St Thomas's Hospital (United Kingdom), and the National Metrology Institute of Turkey (TUBITAK-UME). The calibration methods and radiation sources used by each participant are listed in Table 1.

Table 1. Calibration methods and radiation sources used in the pilot comparison.

Participant	Method	Radiation Source
STUK	SR	Philips TL 100W/WW natural fluorescent sunbed lamp
Univ. of Dundee	SR	Bank of six Philips 100W R tubes
G. & St T Hospital	SIR	Waldmann 7001K phototherapy treatment cabinet
TUBITAK-UME	SIR	Philips TL 20W/05 Actinic UV tube

Figure 21 shows the results of the pilot comparison. The results are given as the relative deviation from the reference value of the comparison. The reference value was calculated as a weighted average of the results of all participants. The weight of each laboratory was determined as $1/u^2$, where u is the relative measurement uncertainty, specified by the participant. The overall spread of the results is ± 5 %, which means a factor of two improvement, compared to the best inter-comparisons performed earlier. [34]
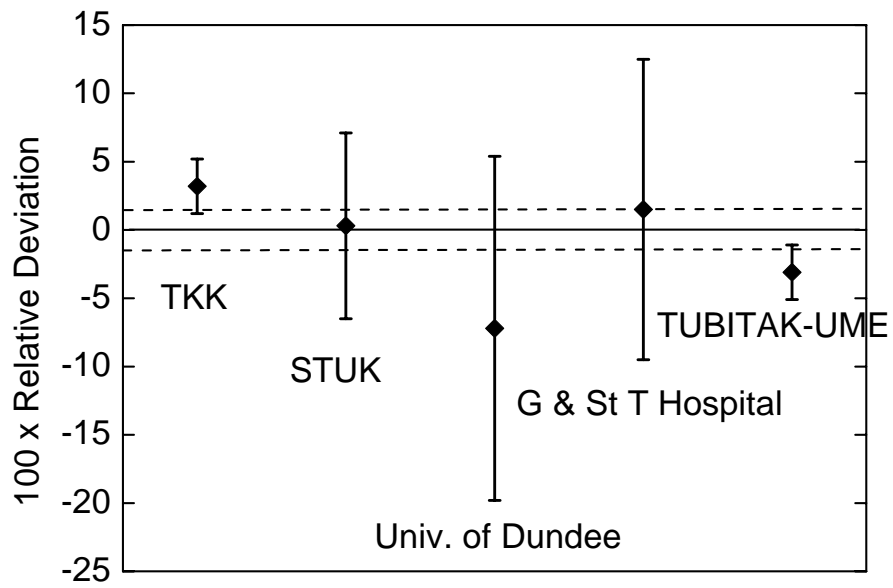
42

Figure 21. Results of the comparison, given as the relative deviation from the reference value. The error bars indicate the measurement uncertainties (*k*=2) specified by each laboratory. The dashed lines denote the uncertainty (*k*=2) of the reference value.

5   Conclusions

In this thesis, measurement standards and methods have been developed for the needs of optical metrology in fiber optics and broadband UV measurements.

The use of a single plain InGaAs photodiode as a reference standard for fiber optic power measurements at 1.3-μm and 1.55-μm wavelength windows has been successfully tested. [Publication I] The design of the detectors is extremely straightforward and cost effective. The radiometric properties of the high-quality photodiodes used in this study proved to be adequate for use in optical metrology. Especially the improved spatial uniformity of the photodiodes has made the use of detectors of this type possible, at least when using single-mode fibers, for which the spatial distribution of the output power is simpler and more easily defined as compared to multi-mode fibers. This is not, however, a serious limitation, since the fibers used in optical communication are mainly single-mode fibers. The measurement uncertainties, 0.9 % (k=2), proved to be low enough for calibration use. Although lower measurement uncertainties can be achieved by use of more complicated detectors and shorter calibration chains, lower uncertainties would benefit quite little in practical calibration work. In practical calibrations, the additional uncertainty components, such as the repeatability of the fiber connection, contribute easily another 0.5 % to the overall uncertainty.

A reference standard, based on the use of an integrating sphere and an InGaAs photodiode, was built and characterized for fiber optic power measurements at power levels up to 200 mW. [Publication II] Further characterizations have expanded the power range of the sphere detector up to 650 mW. The applicability of the relatively low measurement uncertainty, 1.3 % (k=2), of high power fiber optic calibrations was verified in a trilateral comparison between TKK, SP and DFM. The successful inter-comparison was, to the best of our knowledge, the first of its kind in the world. The development of the high-quality reference standard for fiber optic power measurements at ~100-mW power level has proven valuable in the field of non-linear fiber optics. In a recent study at TKK, Lamminpää *et al*. have demonstrated a drop in the measurement uncertainty of the non-linearity coefficient n_2/A_{eff} of optical fibers from 6.4 % to 3.7 % due to the improved measurement capabilities of high power levels. [62] Furthermore, taking into account the effect of dispersion in the measurements, the measurement uncertainty has been lowered down to 2 %. In practice, the lowered measurement uncertainty of the non-linearity coefficient measurements has enabled comparison of the non-linear properties of different fibers. In earlier studies the differences observed were within measurement uncertainties. [17]

The magnitude of the effect of removing the fiber adapter of the sphere detector during the absolute responsivity measurement was determined. [Publication I] The change in the measurement geometry between the calibration and the fiber measurements is known to cause a systematic calibration error. [21, 35] Several ways to deal with the problem have been introduced, but this work was the first time that this effect was actually measured. The result, less than 10^{-3}, was found to be small compared to measurement uncertainties.

44

A spectral comparator facility, utilizing a single grating monochromator and an intense xenon arc lamp, was built and characterized for measurements of $s(\lambda)$ at the UV range. [Publication III] The use of a single grating monochromator was a known risk in order to maximize the output power. By doing this we were able to reach power levels required to have a measurable signal, at a narrow band, out of a broadband UV detector, whose responsivity is typically low. The problem with single grating monochromators is the relatively high level of straylight. The measurements of Publication III, along with further studies [70] have shown that the level of straylight is sufficiently low at the UVA region. We were also able to demonstrate the agreement of SR and SIR methods. This was not the first time this was done [65], but to the best of our knowledge we have done it with considerably lower measurement uncertainties than any other workers.

A novel method was introduced for inter-comparisons of calibration facilities of broadband UV detectors. [Publication IV] The method utilizes the prior knowledge of the $s(\lambda)$ and the angular response of the detector used in the comparison. In addition, the spectral data of all the radiation sources used, and the geometry of each measurement setup are required. Having all these data, the pilot laboratory is able to calculate individual reference values for each participant. The main advantage of this method, compared to other methods used, is that it enables the comparison of different calibration laboratories doing their regular work. Especially, most accredited calibration laboratories have no use for inter-comparisons in which they are required to use a method, for which they do not have accreditation. The method was also found to be insensitive to errors in the spectral shape of the sources used by the participants. The applicability of the method was verified with a pilot comparison of five calibration laboratories. The results of all participants were within ±5 %, which means a factor of two improvement compared to the best earlier comparisons.

References

1. The International System of Units (SI), 7th Edition Bureau International des Poids et Mesures, Sèvres Cedex, France (1998) 72 p.

2. J.W.T. Walsh, *Photometry*, Dover Publications Inc, New York (1958) 544 p.

3. J. Terrien, "News from the International Bureau of Weights and Measures," *Metrologia* **4**, 41-45 (1968).

4. J.E. Martin, N.P. Fox, and P.J. Key, "A Cryogenic Radiometer for Absolute Radiometric Measurements," *Metrologia* **21**, 147-155 (1985).

5. T. Varpula, H. Seppä, and J.-M. Saari, "Optical power calibrator based on a stabilized green He-Ne laser and a cryogenic radiometer," *IEEE Trans. Instrum. Meas*. **38**, 558-564 (1989).

6. A. Lassila, *National standards for dimensional and optical quantities*, Thesis for the degree of Doctor of Technology, Helsinki University of Technology, Metrology Research Institute, Espoo, Finland, 1997.

7. T.R. Gentile, J.M. Houston, and C.L. Cromer, "Realization of a scale of absolute spectral response using the National Institute of Standards and Technology high-accuracy cryogenic radiometer," *Appl. Opt*. **35**, 4392-4403 (1996).

8. J.E. Martin and P.R. Haycocks, "Design considerations for the construction of an absolute radiation detector at the NPL," *Metrologia* **35**, 229-233 (1998).

9. E.F. Zalewski and C.R. Duda, "Silicon photodiode device with 100 % external quantum efficiency," *Appl. Opt*. **22**, 2867-2873 (1983).

10. N.P. Fox, "Trap detectors and their properties," *Metrologia* **28**, 197-202 (1991).

11. T. Kübarsepp, P. Kärhä, and E. Ikonen, "Characterization of polarization independent transmission trap detector, " *Appl. Opt.* **36**, 2807-2812 (1997).

12. T. Kübarsepp, P. Kärhä, and E. Ikonen, "Interpolation of the spectral responsivity of silicon photodetectors in the near ultraviolet," *Appl. Opt.* **39**, 9-15 (2000).

13. Ramaswami and K.N. Sivarajan, *Optical Networks*, Morgan Kaufmann, USA (2002).

14. A.E. Willner, "Minig the optical bandwidth for a terabit per second," *IEEE Spectrum* April 1997, 32-41.

15. R. Gallawa and X. Li, "Calibration of optical fiber power meters: the effect of connectors," *Appl. Opt.* **26**, 1170-1174 (1987).

16. J. Lehman and C. Cromer, "Optical Trap Detector for Calibration of Optical Fiber Powermeters: Coupling Efficiency," *Appl. Opt.* **41**, 6531-6536 (2002).

17. A. Lamminpää, T. Niemi, E. Ikonen, P. Marttila, and H. Ludvigsen, "Effects of dispersion on nonlinearity measurement of optical fibers," *Opt. Fiber Technol.* **11**, 278–285 (2005).

18. R.W. Gilsdorf and J.C. Palais, "Single-mode fiber coupling efficiency with graded-index rod lenses," *Appl. Opt.* **33**, 3440-3445 (1994).

19. J. Lehman and X. Li, "A transfer standard for optical fiber power metrology," *Eng. Lab. Notes Opt. & Photon. News* **10**, (1999), archived in *Appl. Opt.* **38**, 7164-7166 (1999).

20. L.P. Boivin, "Properties of sphere radiometers suitable for high-accuracy cryogenic-radiometer-based calibrations in the near-infrared," *Metrologia* **37**, 273-278 (2000).

21. P. Corredera, J. Campos, M.L. Hernanz, J.L. Fontecha, A. Pons, and A. Corróns, "Calibration of near-infrared transfer standards at optical-fibre communication wavelengths by direct comparison with a cryogenic radiometer," *Metrologia* **35**, 273-277 (1998).

22. A. Carrasco-Sanz, F. Rodríguez-Barrios, P. Corredera, S. Martín-López, M. González-Herráez, and M.L. Hernanz, "An integrating sphere radiometer as a solution for high power calibrations in fibre optics," *Metrologia* **43**, S145-S150 (2006).

23. C.R. Roy, H.P. Gies, D.J. Lugg, S. Toomey, and D.W. Tomlinson, "The measurement of solar ultraviolet radiation," *Mutation Res.* **422**, 7-14 (1998).

24. L. Floyd, K.W. Tobiska, and R.P. Cebula, "Solar UV irradiance, its variation, and its relevance to the Earth," *Adv. Space Res.* **29**, 1427-40 (2002).

25. G. Horneck, "Quantification of the biological effectiveness of environmental UV radiation," *J. Photochem. Photobiol. B: Biol.* **31**, 43-49 (1995).

26. A.A. Abdel-Fattah, M. El-Kelaney, F. Abdel-Rehim, and A.A. El Miligy, "UV-sensitive indicators based on bromophenol blue and chloral hydrate dyed poly(vinyl butyral)," *J. Photochem. Photobiol. A: Chem.* **110**, 291-297 (1997).

27. J. Benrath, F. Gillardon, and M. Zimmermann, "Differential time courses of skin blood flow and hyperalgesia in the human sunburn reaction following ultraviolet irradiation of the skin," *Eur. J. Pain* **5**, 155-167 (2001).

28. H. Oliver and H. Moseley, "The use of diode array spectroradiometers for dosimetry in phototherapy," *Phys. Med. Biol.* **47**, 4411-4421 (2002).

29. H. Kaczmarek, J. Kowalonek, A. Szalla, and A. Sionkowska, "Surface modification of thin polymeric films by air-plasma or UV-irradiation," *Surf. Sci.* **507–510**, 883-888 (2002).

30. T. Larason and Y. Ohno, "Calibration and characterization of UV sensors for water disinfection," *Metrologia* **43**, S151-S156 (2006).

31. A.F. McKinley and B.L. Diffey, "A reference action spectrum for ultraviolet induced erythema in human skin," *CIE Res. Note, CIE-Journal* **6**, 17-22 (1987).

32. G. Xu and X. Huang, "Characterization and calibration of broadband ultraviolet radiometers," *Metrologia* **37**, 235-242 (2000).

33. G. Xu and X. Huang, "Calibration of broadband UV radiometers – methodology and uncertainty evaluation," *Metrologia* **40**, S21-S24 (2003).

34. J.J. Lloyd, "Initial Survey of UV Meter Calibration Centres," *UVNews* **5**, 38-41 (2000). Available on-line at http://metrology.tkk.fi/uvnet/ (11.4.2006).

35. D.H. Nettleton, "Application of absolute radiometry to the measurement of optical power in fibre optic systems," *Inst. Phys. Conf. Ser.* **92**, 93-97 (1989).

36. R.W. Whatmore, "Pyroelectric devices and materials," *Rep. Prog. Phys.* **49**, 1335-1386 (1986).

37. I. Mellouki, O. Touayar, T. Ktari, F. Saadallah, J. Bastie, and N. Yacoubi, "Study and realization of a trap pyroelectric detector for absolute high radiant powers and energies," *Meas. Sci. Technol.* **15**, 384–388 (2004).

38. J. Lehman, G. Eppeldauer, J. A. Aust, and M. Racz, "Domain-engineered pyroelectric radiometer," *Appl. Opt.* **38**, 7047-7055 (1999).

39. J. Conradi, "Planar germanium photodiodes," *Appl. Opt.* **14**, 1948-1952 (1975).

40. T. Saito, K. Katori, M. Nishi, and H. Onuki, "Spectral quantum efficiencies of semiconductor photodiodes in the far ultraviolet region," *Rev. Sci. Instrum.* **60**, 2303-2306 (1989).

41. N.P. Fox, "Improved near-infrared detectors," *Metrologia* **30**, 321-325 (1993).

42. K.D. Stock and R. Heine, "Spectral characterization of InGaAs trap detectors and photodiodes used as transfer standards," *Metrologia* **37**, 449-452 (2000).

43. J. Envall, *Spektrisen irradianssivasteen kalibrointilaitteisto ultraviolettialueen radiometreille*, Thesis for the degree of Master of Science in Technology, Helsinki University of Technology, Metrology Research Institute, Espoo, Finland, 2003. (in Finnish)

44. J. Sinkkonen, *Puolijohdeteknologian perusteet*, Reports in Electron Physics 1996/11, Otaniemi (1996). (in Finnish)

45. P. Kärhä, *Trap detectors and their applications in the realisation of spectral responsivity, luminous intensity, and spectral irradiance scales*, Thesis for the degree of Doctor of Technology, Helsinki University of Technology, Metrology Research Institute, Espoo, Finland, 1997.

46. M. Noorma, *Development of detectors and calibration methods for spectral irradiance and radiometric temperature measurements*, Thesis for the degree of Doctor of Science in Technology, Helsinki University of Technology, Metrology Research Institute, Espoo, Finland, 2005.

47. P. Kärhä, P. Toivanen, F. Manoochehri, and E. Ikonen, "Development of a detector-based absolute spectral irradiance scale in the 380–900-nm spectral range," *Appl. Opt.* **36**, 8909-8918 (1997).

48 R. Kohler, R. Goebel, R. Pello, and J. Bonhoure, "Effects of Humidity and Cleaning on the Sensitivity of Si Photodiodes," *Metrologia* **28**, 211-215 (1991).

49. T. Kübarsepp, *Optical Radiometry using Silicon Photodetectors*, Thesis for the degree of Doctor of Technology, Helsinki University of Technology, Metrology Research Institute, Espoo, Finland, 1999.

50. G.P. Agrawal, *Non-linear Fiber Optics*, Academic Press, USA (2001).

51. Cisco Systems, Inc. Introduction to DWDM for metropolitan networks. Cisco Systems Documentation, 2000. Available online at http://www.cisco.com/univercd/cc/td/doc/product/mels/cm1500/dwdm/ (11.4.2006).

52. J.C. Maxwell, *A treatise on electricity and magnetism*, 3rd edition, Clarendon press, Oxford (1904).

53. E. Desurvire, J.R. Simpson, and B.C. Becker, "High-gain erbium-doped traveling-wave fiber amplifier," O*pt. Lett.***12**, 888-890 (1987).

54. Internet pages of Electrical, Computer, and Systems Engineering Department of Rensselaer Polytechnic Institute: http://www.ecse.rpi.edu/~schubert/Light-Emitting-Diodes-dot-org/MaterialsIII.pdf (11.4.2006).

55. R.E. Nahory, M.A. Pollack, and W.D. Johnston Jr., "Band gap versus composition and demonstration of Vegard's law for $In_{1-x}Ga_xAs_yP_{1-y}$ lattice matched to InP," *Appl. Phys. Lett.* **33**, 659-661 (1978).

56. D.W. Palmer, www.semiconductors.co.uk, 2001 (11.4.2006).

57. Personal communication with Mart Noorma.

58. *A guide to integrating sphere theory and applications*, available on-line at the internet pages of Labsphere Inc. http://www.labsphere.com (11.4.2006).

59. Gigahertz-Optik GmbH, *Application & Product Guide 2004*.

60. Labsphere Inc., *Sphere systems and Instrumentation, Catalog II* (1997).

61. J. Envall, *National standard for fiber optic power*, Thesis for the degree of Licentiate of Science in Technology, Helsinki University of Technology, Metrology Research Institute, Espoo, Finland, 2005.

62. A. Lamminpää, T. Hieta, J. Envall, and E. Ikonen, "Uncertainty contributions related to dispersion and power measurement in determination of fiber nonlinearity using CW SPM method," *Opt. Express* (submitted).

63. G. Xu, X. Huang, and Y. Liu, "Area correction in the calibration of detectors for ultraviolet radiation measurement," *Metrologia* **37**, 559-562 (2000).

64. T.C. Larason and C.L. Cromer, "Sources of error in UV radiation measurements," *J. Res. Natl. Inst. Stand. Technol.* **106**, 649-656 (2001).

65. A.J. Coleman, M. Collins, and J.E. Saunders, "Traceable calibration of ultraviolet meters used with broadband, extended sources," *Phys. Med. Biol.* **45**, 185-196 (2000).

66. T.C. Larason, S.W. Brown, G.P. Eppeldauer, and K.R. Lykke, "Responsivity calibration methods for 365-nm irradiance meters," *IEEE Trans. Instrum. Meas.* **50**, 474-477 (2001).

67. S.D. Pye and C.J. Martin, "A study of the directional response of ultraviolet radiometers: I. Practical evaluation and implications for ultraviolet measurement standards," *Phys. Med. Biol.* **45**, 2701–2712 (2000).

68. P. Manninen, J. Hovila, L. Seppälä, P. Kärhä, L. Ylianttila, and E. Ikonen, "Determination of distance offsets of diffusers for accurate radiometric measurements," *Metrologia* **43**, S120-S124 (2006).

69. G. Xu, X. Huang, and Y. Liu, "APMP PR-S1 comparison on irradiance responsivity of UVA detectors," in *Abstracts of NEWRAD2005*, 9th International Conference on New Developments and Applications in Optical Radiometry, Davos, Switzerland, October 17–19, 2005, p. 237-238.

70. J. Envall, B.C. Johnson, P. Kärhä, T. Larason, and E. Ikonen, "Comparison of spectral irradiance responsivity scales of TKK and NIST in the UVA region," in *Abstracts of NEWRAD2005*, 9th International Conference on New Developments and Applications in Optical Radiometry, Davos, Switzerland, October 17–19, 2005, p. 147-148.